Geochimica et Cosmochimica Acta, Vol. 69, No. 15, pp. 3813–3829, 2005

0016-7037/05 $30.00 + .00

doi:10.1016/j.gca.2005.01.019

Trace sulfate in mid-Proterozoic carbonates and the sulfur isotope record of biospheric evolution

Anne M. Gellatly and Timothy W. Lyons*,†
Department of Geological Sciences, University of Missouri, Columbia, MO 65211, USA

(*Received February* 6, 2004; *accepted in revised form January* 10, 2005)

Abstract—Concentrations of oceanic and atmospheric oxygen have varied over geologic time as a function of sulfur and carbon cycling at or near the Earth's surface. This balance is expressed in the sulfur isotope composition of seawater sulfate. Given the near absence of gypsum in pre-Phanerozoic sediments, trace amounts of carbonate-associated sulfate (CAS) within limestones or dolostones provide the best available constraints on the isotopic composition of sulfate in Precambrian seawater. Although absolute CAS concentrations, which range from those below detection to ~120 ppm sulfate in this study, may be compromised by diagenesis, the sulfur isotope compositions can be buffered sufficiently to retain primary values.

Stratigraphically controlled $\delta^{34}S$ measurements for CAS from three mid-Proterozoic carbonate successions (~1.2 Ga Mescal Limestone, Apache Group, Arizona, USA; ~1.45–1.47 Ga Helena and Newland formations, Belt Supergroup, Montana, USA; and ~1.65 Ga Paradise Creek Formation, McNamara Group, NW Queensland, Australia) show large isotopic variability (+9.1‰ to +18.9‰, −1.1‰ to +27.3‰, and +14.1‰ to +37.3‰, respectively) over stratigraphic intervals of ~50 to 450 m. This rapid variability, ranging from scattered to highly systematic, and overall low CAS abundances can be linked to sulfate concentrations in the mid-Proterozoic ocean that were substantially lower than those of the Phanerozoic but higher than values inferred for the Archean. Results from the Belt Supergroup specifically corroborate previous arguments for seawater contributions to the basin. Limited sulfate availability that tracks the oxygenation history of the early atmosphere is also consistent with the possibility of extensive deep-ocean sulfate reduction, the scarcity of bedded gypsum, and the stratigraphic $\delta^{34}S$ trends and ^{34}S enrichments commonly observed for iron sulfides of mid-Proterozoic age.

1. INTRODUCTION

The biogeochemical cycles of sulfur and carbon are linked through biotic and abiotic processes at and near the Earth's surface and have been responsible in part for modulating oxygen concentrations in the ocean and atmosphere over geologic time (Berner, 1982; Schidlowski, 1983; Holland, 1999). Throughout the Phanerozoic, interactions between carbon and sulfur are expressed as broad shifts in the sulfur isotope composition of seawater sulfate recorded in gypsum deposits and in the carbon isotope composition of whole-rock and skeletal sedimentary carbonates (Claypool et al., 1980; Strauss, 1993; Veizer et al., 1999). Given the near absence of gypsum in pre-Phanerozoic sediments and the unexplored but likely limited potential of the marine (biogenic) barite proxy in very ancient, rapidly accumulating shallow-water carbonates (compare Paytan et al., 1998, 2004, for Phanerozoic examples), recent Precambrian studies are utilizing trace amounts of carbonate-associated sulfate (CAS) within limestone or dolostone as a proxy for seawater sulfate. Because sulfate accumulation in the ocean is largely a product of oxidative weathering of the continents, CAS trends in mid-Proterozoic rocks are critical to our understanding of the rise of atmospheric oxygen, associated eukaryotic and bacterial diversification, and linkages to tectonic reorganization.

This study focuses on carbonates from three mid-Proterozoic successions: ~1.2 Ga (billion year old) rocks of the Apache Group, United States; the ~1.4–1.5 Ga Belt Supergroup, United States; and the ~1.6–1.7 Ga McNamara Group, Australia. Carbonate-associated sulfate in stratigraphically controlled samples from each succession was analyzed for its concentration and $^{34}S/^{32}S$ ratio. Our results show wide variations in sulfur isotope signatures and sulfate concentrations ranging from values below detection to ~120 ppm. These data help fill critical gaps in the record of mid-Proterozoic seawater sulfate chemistry. They also further corroborate the utility of the CAS method in Precambrian studies and, collectively, point to limited sulfate availability in the Proterozoic ocean.

2. BACKGROUND

2.1. Sulfur Biogeochemistry

During the first step of sedimentary pyrite formation, sulfate-reducing bacteria preferentially reduce the light isotope (^{32}S) and leave the resultant sulfate reservoir enriched in the heavier isotope (^{34}S). Consequently, the S isotope composition of bacteriogenic pyrite varies with the kinetic isotope effect during reduction, yielding maximum observed depletions in ^{34}S of 40–45‰ (Harrison and Thode, 1958; Kaplan and Rittenberg, 1964; Kemp and Thode, 1968; Chambers et al., 1975; Chambers and Trudinger, 1979; Habicht and Canfield, 1997, 2001; Canfield, 2001; Detmers et al., 2001). Because ^{34}S depletions of up to 70‰ have been reported in modern environments and cannot easily be explained by microbial sulfate reduction alone, additional fractionation has been attributed to

* Author to whom correspondence should be addressed (timothy.lyons@ucr.edu).
† Present address: Department of Earth Sciences, University of California, Riverside, CA 92521 USA.

redox cycling and associated disproportionation reactions (Canfield and Thamdrup, 1994; Canfield and Teske, 1996; Habicht and Canfield, 1996, 1997, 2001; Habicht et al., 1998; compare Wortmann et al., 2001). Depending on the reservoir properties (e.g., sulfate availability; Zaback et al., 1993); the redox state of the system, including pathways of oxidation/disproportionation; and the initial kinetic controls, such as sulfate reduction rates (Detmers et al., 2001; Canfield, 2001; Habicht and Canfield, 2001), bacteriogenic pyrite can display broad isotopic ranges that include both strongly positive $\delta^{34}S$ values and large ^{34}S depletions relative to the parent sulfate.

Because sedimentary pyrite is commonly depleted in ^{34}S, particularly during the Phanerozoic, variability in the sulfur isotope composition of oceanic sulfate can be used to track the balance between pyrite burial and weathering (Berner and Raiswell, 1983). In the Phanerozoic, this well-studied cycle is expressed in $\delta^{34}S$ trends observed in the gypsum/anhydrite record (Claypool et al., 1980), as well as in marine (biogenic) barite (Paytan et al., 1998, 2004) and CAS (Kampschulte and Strauss, 2004). In the Precambrian, the complex pathways of sulfur cycling and associated S isotope effects are less well known because of the comparative scarcity of gypsum/anhydrite deposits and the growing but still limited use of the CAS proxy.

2.2. Precambrian History of $\delta^{34}S$

A recent study argued for the appearance of bacterial sulfate reduction by at least 3.47 Ga (Shen et al., 2001). The possible onset of this metabolic innovation indicates the presence of sulfate within the Archean ocean, although $\delta^{34}S$ values for nonhydrothermal, Archean sedimentary sulfides typically cluster close to 0‰ and have been attributed to bacterial processing under very low sulfate conditions, perhaps less than 200 μM, in an oxygen-deficient world (Canfield, 1998; Canfield et al., 2000; Habicht et al., 2002). Although controversial, other investigators have suggested instead that the Archean to earliest Proterozoic ocean/atmosphere was largely oxic and that the small apparent isotopic offsets between coeval sulfate and sulfide imply very high rates of bacterial sulfate reduction in an ocean with abundant sulfate availability (Ohmoto and Felder, 1987; Ohmoto et al., 1993; Kakegawa et al., 1998; Lasaga and Ohmoto, 2002; compare Habicht and Canfield, 1996; Canfield et al., 2000). Unfortunately, arguments regarding Precambrian S isotope trends are based primarily on sedimentary pyrite with minimal constraint on coeval sulfate relationships. The details of the available data and the critical debates are reviewed in Lyons et al. (2004b), which also provides a general overview of the Precambrian sulfur isotope record.

Although not universally accepted, the prevailing opinion argues that by ~2.3–2.4 Ga, the so-called Great Oxidation Event marked the transition from fundamentally reducing to oxidizing conditions at the Earth's surface (Holland, 2002; Bekker et al., 2004). This event is expressed in a variety of proxy records, including the mass-independent behavior of sulfur isotopes (Farquhar et al., 2000; Farquhar and Wing, 2003; Bekker et al., 2004) and a broadening of the $\delta^{34}S$ values of pyrite in fine-grained siliciclastic sediments (Canfield, 1998; Shen et al., 2001). In the presence of a non-sulfate-limited ocean, bacteria were able to fractionate sulfur to values governed by the kinetic isotope effect (Canfield, 2001; Detmers et al., 2001). However, the precise magnitude of this fractionation in the Precambrian is difficult to assess given the paucity of coeval sulfate S isotope data—the baseline against which the pyrite data are compared. Furthermore, although no longer sulfate-limited in terms of overall availability to bacteria and the associated kinetic isotopic offset at the cellular level, a Proterozoic ocean with appreciably lower sulfate than the Phanerozoic would remain more vulnerable to reservoir-scale ^{34}S enrichment expressed in the bulk pyrite pool.

By roughly 0.8 Ga, fractionations between sulfate and sulfide appear to have increased to values consistent with those observed throughout the Phanerozoic (up to and exceeding 60–70‰), which are often greater than the ~45‰ possible by bacterial sulfate reduction alone. This increase may record an additional step in oxygen production that supported nonphotosynthetic bacterial oxidation of sulfide and disproportionation of the resulting intermediate S species (Canfield and Thamdrup, 1994; Canfield and Teske, 1996; Canfield, 1998). Repeated redox cycling could have driven S isotope offsets between parent sulfate and product sulfide to the large values observed during the latest Precambrian and Phanerozoic. Alternatively, Hurtgen et al. (2005) argued that disproportionation reactions were likely a factor throughout the Proterozoic, but fractionations did not exceed ~45‰ before ~580 Ma because of the low sulfate concentrations in seawater and efficient burial of pyrite. In this case, larger apparent fractionations may instead be an artifact of high $\delta^{34}S_{sulfate}$ variability, yielding a broad range of $\delta^{34}S_{pyrite}$ values over a narrow stratigraphic interval even in the presence of comparatively small net fractionation. In either case, actual expanded fractionations in the middle or late Neoproterozoic could simply reflect increasing seawater sulfate concentrations (Kah et al., 2004; Lyons et al., 2004b; Hurtgen et al., 2005; this study) driven by increasing biospheric pO_2 in response to organic carbon burial and the second major episode of Earth surface oxygenation (Des Marais et al., 1992; Canfield and Teske, 1996; Des Marais, 1997; Canfield, 1998). A late Neoproterozoic (post-Marinoan glaciation) rise in oxygen—perhaps expressed in the sulfur isotope record—would have set the stage for metazoan evolution (Hurtgen et al., 2005). Despite the complexities and multiple controls on sulfur cycling and the related isotope and concentration relationships at the Earth's surface (Canfield, 2005), patterns of sulfate chemistry in the early ocean may still be our best quantitative tracer of biospheric oxygenation. Nevertheless, the amount and isotopic composition of sulfate in the Proterozoic ocean remain poorly known.

Gypsum formed during seawater evaporation has traditionally been used to constrain the secular isotopic evolution of oceanic sulfate over the last ~500 million years (Holser and Kaplan, 1966; Claypool et al., 1980; Strauss, 1993, 1997, 1999; Strauss et al., 2001). Sulfur is only slightly fractionated (<2‰) during gypsum precipitation and thus, when formed in marine settings, approximates the $\delta^{34}S$ of seawater sulfate. Unfortunately, gypsum (being soluble and vulnerable to weathering) has poor preservation potential, and gypsum saturation is less likely to have occurred under the comparatively lower sulfate conditions of the Archean and Proterozoic (Kah et al., 2001). As a result, gypsum and associated anhydrite are rare in Precambrian sequences.

2.3. Carbonate-Associated Sulfate

2.3.1. Systematics

In the absence of evaporite deposits, sulfate trapped within carbonate rocks has potential for yielding continuous, high-resolution $\delta^{34}S$ records with strong chronostratigraphic context (Burdett et al., 1989; Strauss, 1997; Kampschulte et al., 2001; Hurtgen et al., 2002) and may be the only option available for much of the Precambrian. A number of workers have investigated the geochemical and paleoenvironmental utility of CAS, which commonly occurs at concentrations of $\sim 10^2$ to 10^3 ppm or greater in younger sediments (Busenberg and Plummer, 1985; Takano, 1985; Burdett et al., 1989; Staudt and Schoonen, 1995; Strauss, 1997, 1999; Kampschulte and Strauss, 2004). CAS appears to be dominated by lattice-bound sulfate, which is incorporated through substitution for the carbonate ion despite sulfate's larger size and the structural differences between the two ions (Burdett et al., 1989; Staudt and Schoonen, 1995, and references therein).

Staudt and Schoonen (1995) reported concentrations of CAS in modern carbonates that ranged from less than 1000 ppm to anomalously high values of up to 24,000 ppm. Typical values were in the 1000 to 10,000 ppm range, which is more than adequate for routine S isotope analyses. Recent results corroborate this range. Specifically, mean CAS concentrations of 1610 and 2988 ppm were reported for a variety of skeletal grains from Heron Island, Great Barrier Reef, Australia, and bulk aragonitic muds from Florida Bay, United States, respectively (Lyons et al., 2004c). However, ancient dolomite and calcite often have appreciably lower sulfate concentrations compared to modern skeletal carbonates and bulk carbonate muds.

2.3.2. CAS Isotope and concentration relationships as paleoceanographic proxies

The important study of Burdett et al. (1989) demonstrated that trace sulfate can record the sulfur isotope composition of contemporaneous seawater sulfate. This result was based on analyses of modern bivalves and foraminifera, as well as Miocene foraminifera for which high-resolution evaporite data were also available. Consistent with Burdett et al. (1989), data from Lyons et al. (2004c) for skeletal grains from the Great Barrier Reef, Australia (mean + 20.5‰, $n = 10$) and aragonitic muds from South Florida (mean + 19.5‰, $n = 15$) show CAS isotope values ($\delta^{34}S_{CAS}$) that fall within ~1‰ of modern seawater sulfate (~+21‰, Rees et al., 1978; Longinelli, 1989). Kampschulte et al. (2001) and Kampschulte and Strauss (2004) also reported a strong match between $\delta^{34}S_{CAS}$ in skeletal grains and sulfate in modern seawater. The seawater-like $\delta^{34}S$ values within the bulk mud samples from South Florida are particularly relevant because one of the two localities tested had sediments characterized by high rates of sulfate reduction. The associated increase in alkalinity drove diagenetic calcium carbonate precipitation in the presence of a highly evolved porewater sulfate reservoir (Walter and Burton, 1990; Walter et al., 1993). Despite net $CaCO_3$ precipitation, the $\delta^{34}S_{CAS}$ value is still dominated by primary sediment inputs recording the chemistry of the overlying water (Lyons et al., 2004c).

Although these results are encouraging, diagenesis remains a concern—as for any geochemical proxy preserved in carbonate rocks—and could be the source of some of the isotopic scatter reported here. In an ongoing investigation of CAS relationships in modern and near-modern carbonates sediments and rocks in South Florida designed to explore secondary effects, Lyons et al. (2004a) described CAS concentrations that decreased by almost an order of magnitude (from 3500 to 500 ppm) in response to the inversion of primary aragonite within the coralline Key Largo Limestone to secondary calcite under meteoric diagenetic conditions. Across this same transition, however, the $\delta^{34}S_{CAS}$ remained within ~1 to 2‰ of the coeval seawater value. As for $\delta^{13}C$ values, even in whole-rock micrites (Saltzman et al., 2000), $\delta^{34}S_{CAS}$ appears to be buffered to initial values during diagenesis, whereas CAS concentrations are more vulnerable to postdepositional alteration. Current efforts are exploring CAS relationships in modern dolomite.

Uptake of CAS varies with carbonate mineralogy and likely with crystal growth rates, as do the relative burial stabilities of these carbonate minerals. These differences, which are linked to the environment in which diagenesis occurred and to whether the ocean favored calcite or aragonite precipitation, should have an appreciable effect on CAS concentration trends. Despite these concerns, Hurtgen et al. (2002, 2004) reported Neoprotoerozoic CAS concentrations that averaged tens of ppm (ranging up to a few hundred) and used the contrast with modern carbonates—which typically range in the thousands of ppm—to suggest ancient sulfate concentrations of roughly 10% of the modern ocean. Perhaps fortuitously, this reduced concentration agrees well with the Proterozoic estimates of Shen et al. (2002, 2003), which were calculated independently based on a model for sulfide accumulation in the Proterozoic McArthur Basin and the ^{34}S enrichments that characterize the associated sediments. Secondary effects aside, fundamental differences between Phanerozoic concentrations, which often range into the thousands of ppm despite many millions of years of burial and exposure to diagenesis, and Proterozoic levels, which are often one to two orders of magnitude lower, may generally track the lower availability of sulfate in the Proterozoic ocean. As further corroboration that primary sulfate concentrations in ancient carbonates may not be completely overprinted during diagenesis, the highest CAS concentrations reported by Staudt and Schoonen (1995) from the rock record derive from ancient dolomites described as "evaporitic." Extrapolating from the conclusions of Hurtgen et al. (2002), Pavlov et al. (2003) invoked lower-than-modern sulfate concentrations in their argument for a persistence, albeit at a reduced level, of the high atmospheric methane concentrations that so strongly influenced the Archean climate.

To date, a number of studies have documented the close match between $\delta^{34}S_{CAS}$ values from skeletal grains and coeval Phanerozoic evaporite deposits (Burdett et al., 1989; Strauss, 1999; Kampschulte et al., 2001; Kampschulte and Strauss, 2004), confirming the potential for preserved primary $\delta^{34}S$ values in ancient CAS. Kampschulte et al. (2001) and Kampschulte and Strauss (2004) extended the general match between CAS and evaporite S isotope results to include data from fine-grained, whole-rock carbonate samples. Most recently, CAS results from whole-rock dolomicrites of the ~1.2 Ga Bylot Supergroup of the Canadian arctic strongly parallel the isotopic trend for interbedded gypsum deposits, with an agreement of roughly 3–5‰ or better (Kah et al., 2001, 2004). These

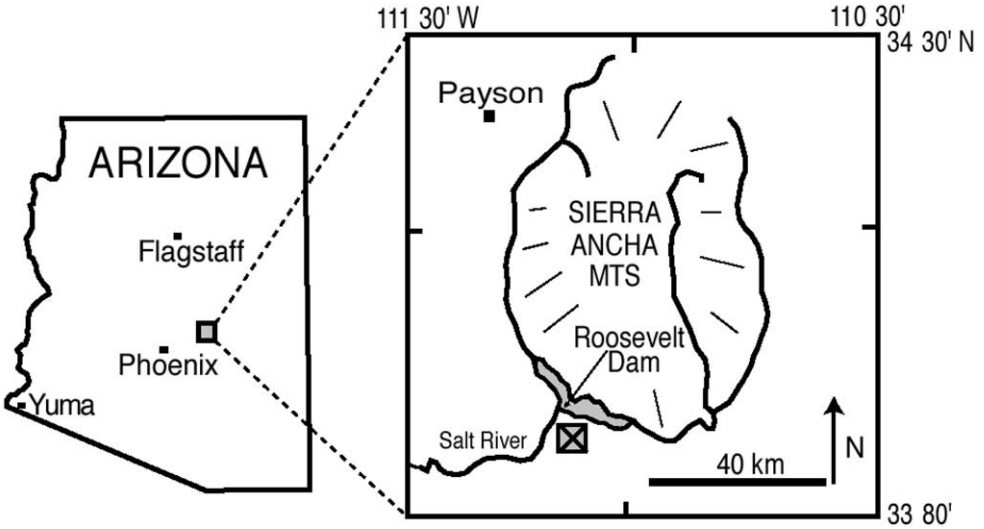

Fig. 1. Map of central Arizona after Beenus and Knauth (1985). Sample locality at Roosevelt Dam is within the algal member of the Mescal Limestone of the Apache Group.

data also suggest that S isotope fractionations during sulfate incorporation into carbonate minerals are typically only a few permil or less and are much smaller than the range of $\delta^{34}S$ variability observed in mid-Proterozoic carbonates. These and other assessments of CAS diagenesis (e.g., Hurtgen et al., 2004) confirm that carbonate rocks, including dolostones, can readily record and preserve the primary $\delta^{34}S$ of sulfate in seawater. CAS concentrations, while likely to be compromised during diagenesis, may at least preserve primary temporal and stratigraphic trends, if not the absolute concentrations.

2.4. Stratigraphy and Regional Geology

2.4.1. Apache Group—Mescal Limestone

The age of the upper Mesoproterozoic Apache Group (Fig. 1) of central Arizona is partially constrained by zircons from tuffaceous beds within the lowermost unit of the Pioneer Shale, which yielded an age of 1.328 Ga (Stewart et al., 2001). Zircons within the Dripping Spring Quartzite and the Troy Quartzite, immediately overlying the Apache Group, have yielded ages of 1.264 and 1.256 Ga, respectively; the zircons in both formations are interpreted to represent volcanism roughly contemporaneous with deposition (Damon et al., 1962; Stewart et al., 2001). The Mescal Limestone (Fig. 2) lies above the Dripping Springs Quartzite and below the Troy Quartzite and consists of four main members (in ascending order): the lower member, the algal member, basalt flows, and the argillite member (Shride, 1967). The Mescal Limestone, which Wrucke (1989) interpreted as a shallow marine deposit, is also intruded by 1100 ± 15 Ma diabase sills and dikes (Silver, 1960, 1978). Collectively, available age controls place the Mescal at ~1.2 Ga (compare Fletcher et al., 2004). The algal member of the Mescal Limestone is ~12–40 m thick and is composed of two main units. The upper unit is a grayish-red to yellowish-brown dolomite with lenses of chert, and the lower algal member is a pale-red to reddish-brown, dolomitized, stromatolitic (*Collenia frequens* and *Baicalia baicalica*) limestone (Bertrand-Sarfati and Awramik, 1992). Although the algal member preserves no primary evaporites, Arthurton (1973) noted gypsum pseudomorphs and molds similar to hopper-shaped halite casts.

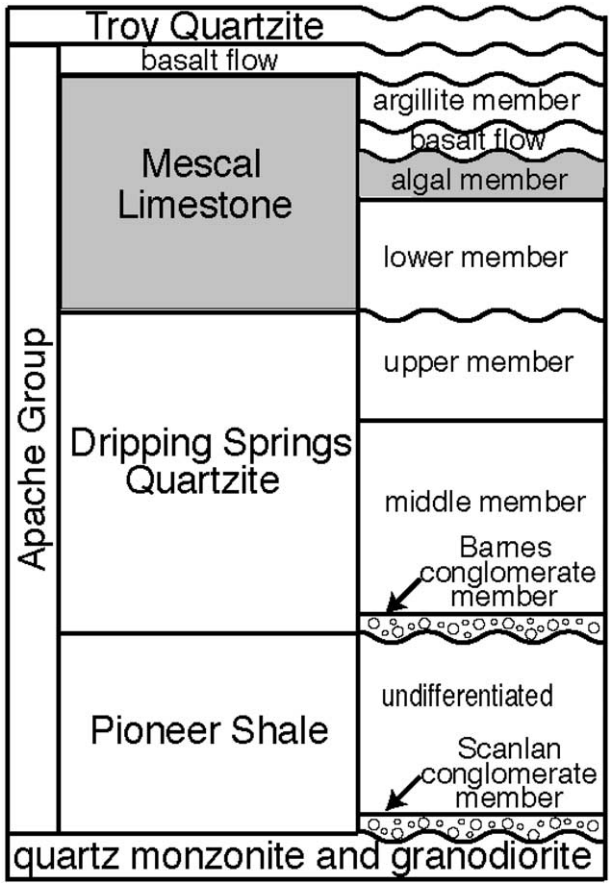

Fig. 2. Generalized stratigraphy of the Apache Group after Shride (1967), Wrucke (1989), and Bertrand-Sarfati and Awramik (1992).

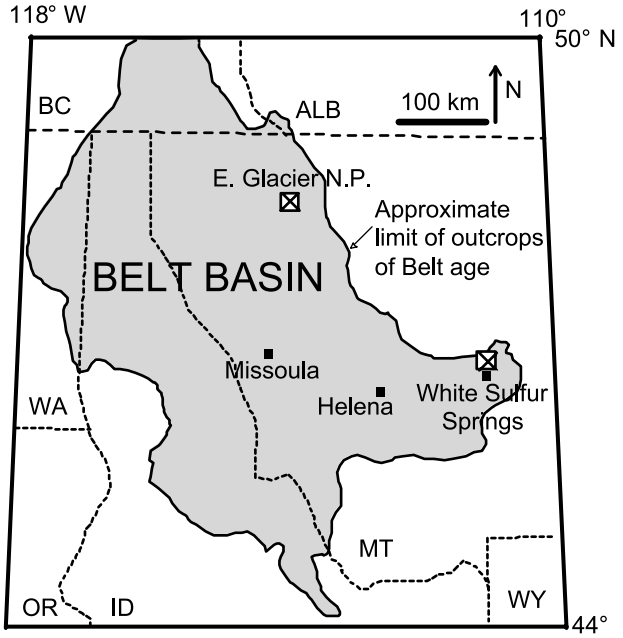

Fig. 3. Map of the Belt Supergroup (after Winston, 1990; Winston and Link, 1993; Luepke and Lyons, 2001). Sample locality [X] near East Glacier National Park is the Ousel Creek section of the Helena Formation. Sample locality near White Sulfur Springs represents three sections of the Newland Formation: Newlan Creek, Zieg Ranch, and Sheep Creek drill core (SC-88; Lyons et al., 2000).

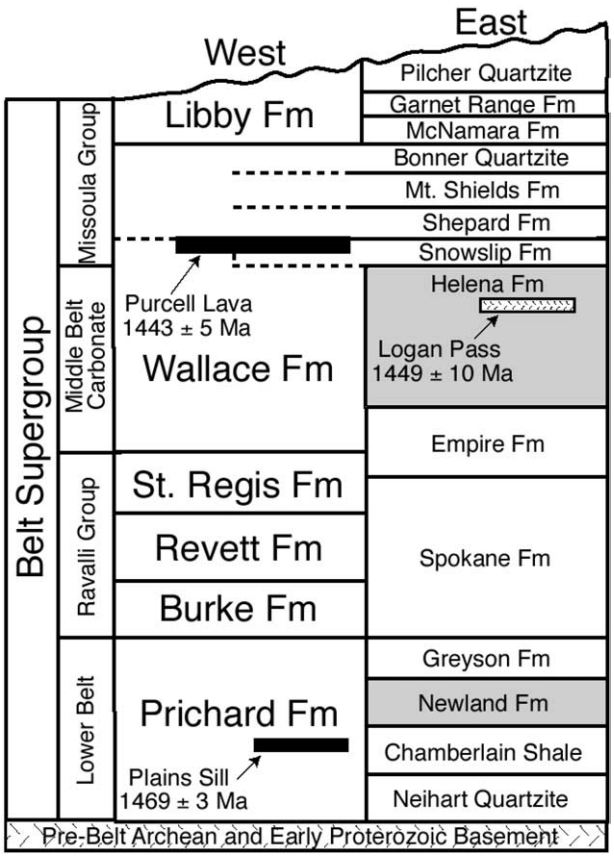

Fig. 4. Generalized stratigraphy of the Belt Supergroup in Idaho and Montana redrawn from Luepke and Lyons (2001). Recent geochronometric ages are discussed in Cressman (1989), Winston and Link (1993), Anderson and Davis (1995), Aleinikoff et al. (1996), and Sears et al. (1998).

2.4.2. Belt Supergroup—Newland and Helena Formations

The Belt Supergroup of the northwestern United States and its Canadian equivalent, the Purcell Supergroup (Fig. 3), are exposed over an area of 130,000 km^2 (Winston, 1990). The Belt Supergroup thickens from ~5 km in the Helena Embayment to ~16 km in the western portion of the Belt basin and was deposited from ~1.47 to 1.37 Ga. Various aspects of the Belt Supergroup, including chronological details, are reviewed in Maxwell and Hower (1967), Harrison (1972), Harrison et al. (1974), Cressman (1989), Winston and Link (1993), and Luepke and Lyons (2001). The lower two-thirds of Belt deposition took place over a period of only 20–30 million years, as constrained by the 1469 ± 3 Ma Plains Sill in the Prichard Formation (Sears et al., 1998), a tuff bed at Logan Pass in the upper part of the Helena Formation (1449 ± 10 Ma), and the Purcell Lava (1443 ± 5 Ma; Aleinikoff et al., 1996).

The Belt Supergroup has been subdivided into four informal units (in ascending order): the lower Belt, Ravalli group, middle Belt carbonate, and Missoula group (Fig. 4). The sedimentology of the Belt Supergroup consists primarily of fine-grained siliciclastic strata and one major carbonate unit (middle Belt carbonate) and has been comprehensively described elsewhere (Harrison, 1972; Harrison et al., 1974; Winston and Link, 1993). Recent results from Lyons et al. (2000) and Luepke and Lyons (2001) challenge earlier assertions of broad temporal- and spatial-scale nonmarine deposition in the Belt basin (Winston, 1990).

2.4.3. McNamara Group—Paradise Creek Formation

The McNamara Group is an upper Paleoproterozoic–lower Mesoproterozoic succession in northwestern Queensland, Australia (Fig. 5). Deposition is constrained between 1678 ± 2 Ma (Carters Bore Rhyolite) and 1595 ± 6 Ma (tuff bed within the Lawn Hill Formation, upper McNamara Group) and is roughly coeval with the McArthur Group and the Mount Isa Group (Page et al., 2000). U-Pb SHRIMP dates are available from zircons in the Fiery Creek Volcanics (1658 ± 3 Ma)—thin, pink tuffaceous layers within the Paradise Creek Formation (Indurm, 2000). The shallow marine McNamara Group (Fig. 6) is represented by ~8500 m of primarily storm deposited and reworked sediments, intraclastic units, quartz and peloid silt and mud, stromatolitic dolomite, and laminated carbonates. Further details are provided in the sequence stratigraphy of Southgate et al. (2000) and Sami et al. (2000).

The Paradise Creek Formation of the lower McNamara Group (~300 m thick) is comprised primarily of interbedded, finely laminated dolomudstone and has been interpreted to represent deeper-water facies deposited mostly below wave base (Blake and Stewart, 1992; Southgate et al., 2000). In the present study, we analyzed stratigraphically controlled carbonate samples from the Paradise Creek Formation at

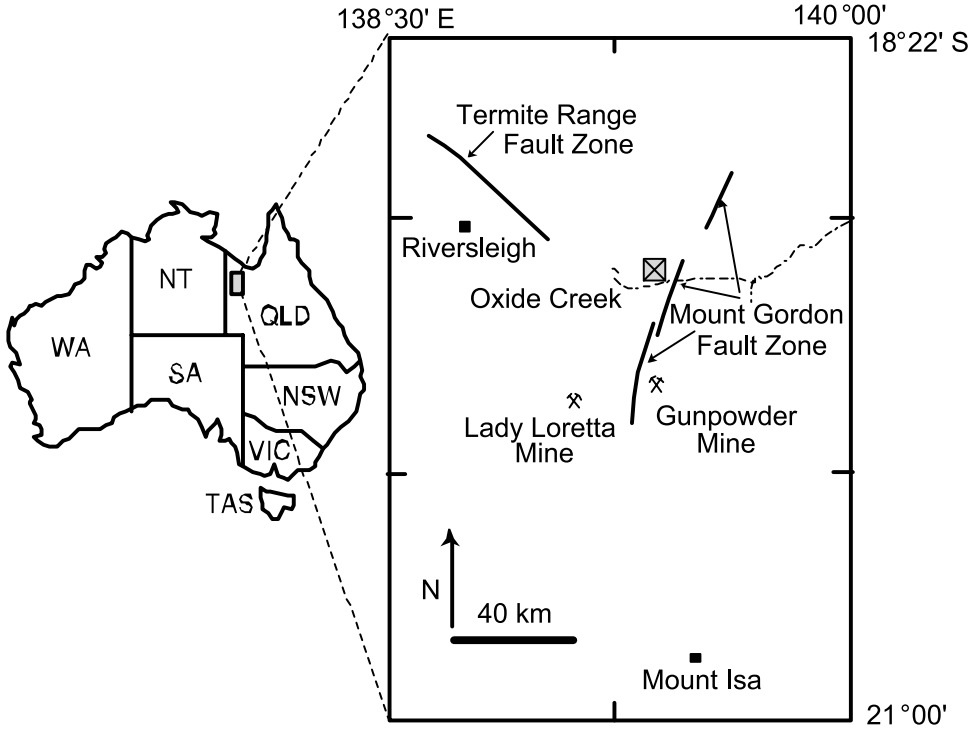

Fig. 5. Map of northwest Queensland, Australia (after Southgate et al., 2000). Sample locality at Oxide Creek is within the Paradise Creek Formation of the lower McNamara Group.

Oxide Creek, starting above the Fiery Creek Volcanics which form the base of the unit (see Southgate et al., 2000, for further details).

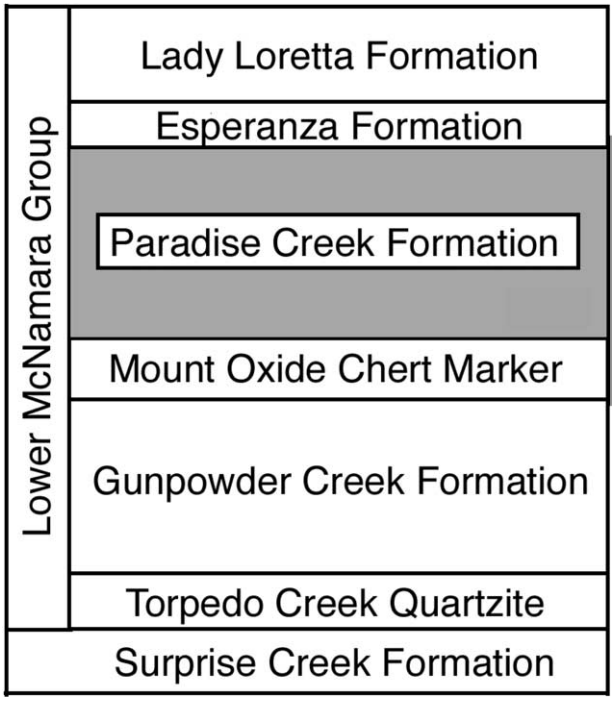

Fig. 6. Generalized stratigraphy of the lower McNamara Group, after Page and Sweet (1998) and Southgate et al. (2000).

3. MATERIALS AND METHODS

3.1. Sample Details

Throughout the study, all carbonates were collected as large hand samples to ensure sufficient sulfate for isotopic analysis. Extreme care was taken during sampling to collect the least weathered materials. More specifically, highly weathered outcrop, secondary veins, and areas of local contact metamorphism were avoided. Furthermore, every effort was made to emphasize carbonate rocks lacking organic matter, appreciable siliciclastic sediment, and diagenetic pyrite.

In Arizona, 13 samples were collected spanning an interval of ~45 m of the algal member of the Mescal Limestone on the south side of the Theodore Roosevelt Dam along the Salt River northeast of Phoenix. The samples span the entire section, although the interval thickness varied as dictated by the distribution of the abundant chert (Table 1). The entire section is strongly dolomitic and stromatolitic. The only obvious lithologic change over the ~45 m of section is the abundance of chert lenses in the upper 15 m; chert is comparatively minor in the lower 30 m.

Limestone samples were collected from the upper Newland Formation, Montana, near White Sulfur Springs (total number of samples = 19: Newlan Creek section, $n = 6$; Zieg Ranch vicinity, $n = 5$; and Sheep Creek drill core [SC-88], $n = 8$) all from within the fault-bounded, unmetamorphosed Helena Embayment. The Newlan Creek samples were taken from a single 2-m outcrop of interbedded limestone and shale. The few Zieg Ranch limestone samples are representative of the lithologies present but were collected without precise stratigraphic context, and the small number of carbonate samples from the SC-88 core were collected at ~60-m intervals.

Large limestone hand samples (~1 kg) from the Helena Formation were collected stratigraphically at ~17-m intervals ($n = 41$) from a well-exposed section along Ousel Creek, Montana. The Ousel Creek section exposes 445 m of dominantly fine-grained, gray weathering micritic limestone. This characteristic Helena Formation locality contains the *Baicalia-Conophyton* stromatolite zone—a distinct lithostratigraphic marker that allows correlation of the Helena Formation over broad regions of the Belt basin (Winston and Link, 1993). The Ousel

Table 1. CAS sulfur isotope compositions and sulfate concentrations (via ICP-OES).

Sample*	$\delta^{34}S_{CAS}$ (‰ V-CDT)	SO_4^{2-} (ppm)
ML 43.0	+18.9	52
ML 40.0	NV	17
ML 35.0	+14.0	BD
ML 34.0	+15.2	34
ML 32.0	+12.3	86
ML 27.0	+9.9	53
ML 25.0	+9.1	40
ML 18.0	+16.5	42
ML 16.0	+16.4	62
ML 15.0	+18.8	42
ML 13.0	+18.8	27
ML 9.0	+11.8	26
ML 4.0	NV	41
HF 445.0	+15.6	116
HF 438.9	+16.6	NV
HF 431.3	+4.7	85
HF 411.5	+14.9	27
HF 399.3	+15.1	BD
HF 387.1	+15.1	54
HF 381.0	−1.1	94
HF 368.8	+3.6	35
HF 353.6	+7.6	56
HF 335.3	+12.6	22
HF 317.0	+9.0	47
HF 307.8	+9.8	9
HF 277.4	+12.0	10
HF 246.9	NV	10
HF 240.8	NV	9
HF 234.7	NV	22
HF 228.6	+13.3	82
HF 222.5	+13.1	25
HF 216.4	+13.0	17
HF 195.1	+18.5	67
HF 189.0	+20.3	93
HF 182.9	NV	11
HF 152.4	NV	9
HF 140.2	+17.8	46
HF 121.9	NV	1
HF 115.8	+13.0	BD
HF 92.4	NV	1
HF 85.3	+14.0	3
HF 79.9	NV	20
HF 73.2	NV	23
HF 59.4	+14.0	11
HF 54.9	NV	18
HF 51.8	+12.7	BD
HF 47.2	+11.9	8
HF 42.7	NV	16
HF 24.4	+10.9	10
HF 22.9	+6.9	10
HF 14.6	NV	9
HF 10.7	NV	3
HF 6.1	+12.0	19
HF 4.6	+11.1	3
SC-88 637.5	+14.0	NV
SC-88 612.2	+19.7	NV
SC-88 581.7	+18.9	NV
SC-88 413.3	+14.4	NV
SC-88 374.9	+15.2	NV
SC-88 320.4	+11.4	NV
SC-88 231.5	+27.3	NV
SC-88 222.3	+17.9	NV
ZR-95-1	+13.7	NV
ZR-95-2	+20.6	NV
ZR-95-3	+22.9	NV
ZR-95-4	+21.1	NV
ZR-95-5	+23.2	NV
NC-12	+23.8	NV
NC-09	+19.7	NV
NC-07	+22.1	NV
NC-05	+12.0	NV
NC-03	+24.6	NV
NC-01	+25.1	NV
PC 546.0	+37.0	NV
PC 545.3	+14.1	74
PC 543.0	+37.3	62
PC 528.0	+30.1	BD
PC 507.0	+30.4	74
PC 502.5	+27.9	BD
PC 486.0	+36.4	62
PC 472.5	+30.6	11
PC 465.0	+37.2	86
PC 462.0	+35.2	91
PC 450.0	+37.2	88
PC 440.6	+35.1	2
PC 430.5	+25.0	92
PC 424.5	+27.4	40
PC 420.0	+30.3	2
PC 411.0	NV	64
PC 405.8	+33.0	92
PC 399.0	+27.8	52
PC 388.5	+31.3	17
PC 384.8	+16.5	22
PC 379.5	+31.5	25
PC 373.5	+32.1	17
PC 368.3	+26.4	10
PC 360.8	+29.0	BD

ML = Mescal Limestone-*Roosevelt Dam;* HF = Helena Formation-*Ousel Creek;* NC = Newland Formation-*Newlan Creek;* SC-88 = Newland Formation-*Sheep Creek Core;* ZR-95 = Newland Formation-*Zieg Ranch;* PC = Paradise Creek Formation; BD = below detection; NV = no value (not measured).

* Sample # refers to stratigraphic thickness in meters.

Creek section contains five shallowing-upward cycles.The uppermost cycle represents a major shallowing event and eventual desiccation and subaerial exposure at the top of the section, expressed by desiccation cracks, intraclasts, flat-pebble conglomerates, cross-beds, and ooids. Based on a small survey of representative samples, total organic carbon content was consistently below 1 wt.%.

In Australia, we sampled a ~185-m section of the Paradise Creek Formation along Oxide Creek north of Mammoth Mines at intervals of ~6 m (n = 24). The section is dominated by fine-grained, microlaminated, dark gray dolomudstone. Replacement evaporite textures and abundant intraclastic beds were observed. Although the sampled portion of the section is lithologically uniform, thick stromatolitic units are present at 436, 517, 521–528, 529–536, and 543–546 m, and thin (1–5 cm) tuff marker beds occur at 366, 372, and 484 m. The top of the Mt. Oxide Chert is at 360 m.

3.2. CAS Preparation

All field samples were trimmed with a water-cooled saw to remove weathered surfaces, powdered, and weighed (100 to 300 g, averaging 202, 184, and 119 g for the Mescal, Helena, and Paradise Creek formations, respectively). The ultimate goal was to ensure sufficient sulfate for isotopic analysis, which varies with instrument sensitivity. Despite challenges intrinsic to any effort to filter and recover small amounts of precipitate, the selected weights were more than adequate in most cases for multiple analyses using ~0.3–0.4 mg of barium sulfate ($BaSO_4$) for each. All laboratory methods were completed at room temperature. Samples were rinsed with deionized water to remove soluble sulfate salts and treated with 5.25% bleach solution

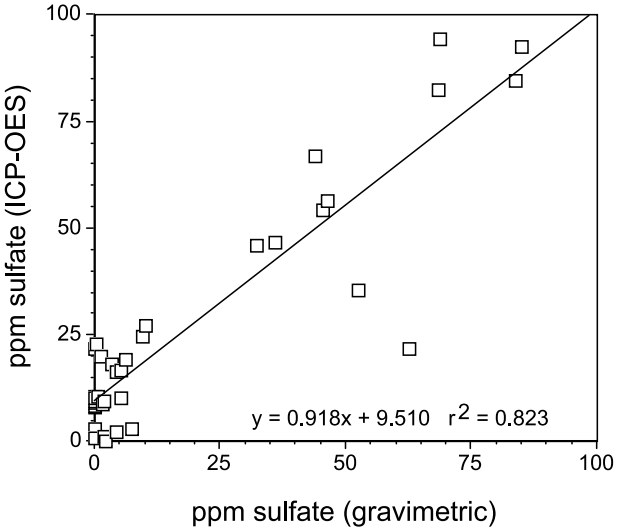

Fig. 7. Comparison of CAS concentrations for the Helena Formation measured by ICP-OES and gravimetric methods. Data are reported as concentrations in the rock samples.

(NaOCl) to remove any organic sulfur, although this step may be unnecessary for the organic-poor samples emphasized in the present study. Samples were then dissolved slowly with 4N HCl to completion and filtered to remove the insoluble residue. The solution was brought to a volume of 1 L, and a 15-mL aliquot was removed for determinations of sulfate concentrations. Trace sulfate was precipitated as $BaSO_4$ by addition of 125 mL of saturated barium chloride ($BaCl_2$) solution (~250 g/L). The $BaSO_4$ precipitate was filtered following room temperature precipitation after 14 days or less. The solution was commonly clear by the second day, with the $BaSO_4$ visibly settled to the bottom. We could then filter confidently as early as the third day.

Stable sulfur isotope analyses were conducted at Indiana University (Bloomington). Barium sulfate precipitates were homogenized, combined with an excess of V_2O_5, and analyzed using a Finnigan MAT 252 gas source mass spectrometer fitted with an elemental analyzer for on-line sample combustion. The sensitivity of this instrument allows for high-precision $\delta^{34}S$ measurements of very small samples (<0.5 mg of pure $BaSO_4$). All sulfur isotope compositions are expressed in standard delta notation as permil (‰) deviations from Vienna Canyon Diablo Troilite (V-CDT), with an analytical error of ± 0.2‰.

Sulfate concentrations were measured at the University of Missouri using a Perkin Elmer inductively coupled plasma–optical emission spectrometer (ICP-OES) fitted with a micro-concentric nebulizer and calibrated through a series of standard solutions and repetitive sample runs. Certified reference materials were used for calibration, and standards were prepared with 0.4N HCl and 5000 ppm calcium solution to simulate a 10-fold diluted sample matrix. Multiple replicates were run, and the detection limit was calculated at 0.7 ppm (sulfate) solution concentration, although recent work suggests that typical detection limits might be higher, with some sensitivity to the strength of the acid matrix (Shim, 2004).

We tested the reliability of the ICP-OES approach by duplicate measurement of sulfate concentrations using gravimetric methods (as $BaSO_4$). The agreement between the two methods is generally good (Fig. 7; also Lyons et al., 2004c; Shim, 2004). However, this comparison illuminates the greater overall sensitivity of the ICP-OES method, particularly for the low concentrations. Because of this agreement but the greater sensitivity of the dissolved sulfate analysis (Shim, 2004), only the ICP-OES data are reported in Table 1 and Figures 8, 9b, 10b, and 11b.

4. RESULTS

The data for all four of the units studied are presented in Table 1 and Figures 8–12. The Mescal Limestone (Roosevelt Dam section) in central Arizona shows a wide range of $\delta^{34}S_{CAS}$ values (Fig. 12a; range: +9.1‰ to +18.9‰, n = 11, mean = +14.7‰), with the suggestion of systematic stratigraphic variability, particularly in the upper half of the section (Fig. 9a). CAS concentrations range from those below detection to 86 ppm (mean = 44 ppm; Fig. 8a) but do not display distinct stratigraphic trends (Fig. 9b).

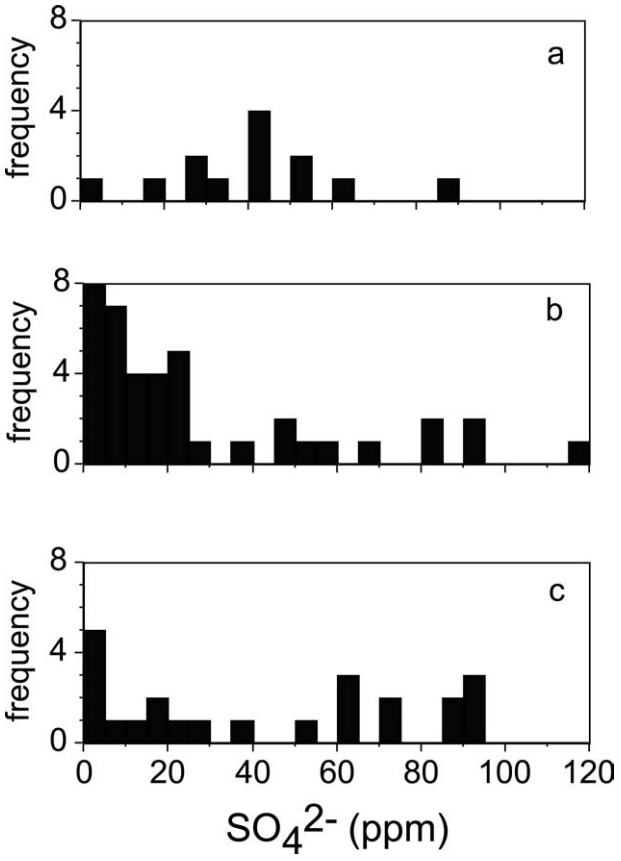

Fig. 8. CAS concentrations for the (a) Mescal Limestone, Apache Group, central Arizona; (b) Helena Formation, Belt Supergroup, Montana; and (c) Paradise Creek Formation, McNamara Group, northwest Queensland.

CAS isotope measurements from the Belt Supergroup Helena Formation (Ousel Creek section) range from −1.1‰ to +20.3‰ (n = 28, mean = +12.1‰, Fig. 12b). After an up-section increase in $\delta^{34}S_{CAS}$ in the lower part of the section, the data shift toward lighter values and then increase sharply at the top of the section (Fig. 10a). This type of systematic variation is of interest because the large changes (~19‰) span only ~380 m of section. Overlying this trend, the dramatic shift at the top the section occurs in association with abundant ooids, crossbeds, and mudcracks. CAS concentrations from the same Ousel Creek Helena samples range from those below detection to 116 ppm (Fig. 8b). Concentrations of CAS at the base of the unit are generally lower than the mean of 30 ppm. Major increases in CAS concentrations occur roughly coincident with a shallowing-upward cycle at ~190 to 230 m and most significantly at the top of the section (~380 to 445 m, with some suggestion of an increase just below this interval, Fig. 10b). These concentration maxima correspond in a very general way

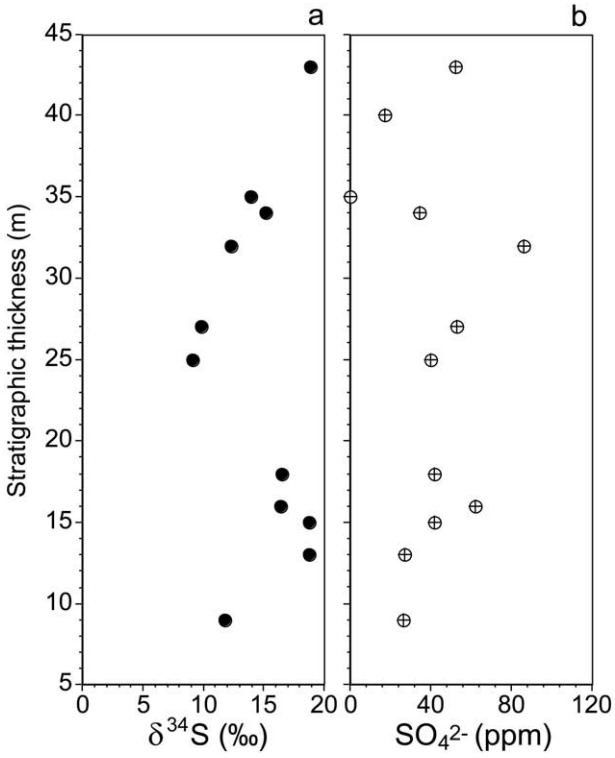

Fig. 9. Roosevelt Dam section of the Mescal Limestone, Apache Group, central Arizona: (a) sulfur isotope compositions ($\delta^{34}S_{CAS}$) and (b) CAS concentrations (ppm sulfate). The section is dominated by relatively uniform stromatolitic dolostone, with chert content increasing in the upper ~15 m (see text for details).

with the isotopic maxima, although the two data sets show few signs of true covariation.

Our values for $\delta^{34}S_{CAS}$ from dolomites of the Belt Supergroup Newland Formation range from +11.4‰ to +27.3‰ (n = 19, mean = +19.4‰, Fig. 12c). Detailed stratigraphic trends were not the goal of this sample set. Instead, we explored the overall range of CAS values relative to past sulfur isotope data from lower Belt barite and iron sulfides (Lyons et al., 2000; Luepke and Lyons, 2001). CAS concentrations are not available for these samples.

The Paradise Creek Formation shows a wide $\delta^{34}S_{CAS}$ range from +14.1‰ to +37.3‰ (n = 23, mean = +30.4‰, Fig. 12d). Stratigraphic variation is less systematic than that observed in the Helena data, although subtle trends may be present (Fig. 11a). CAS concentrations range from levels below detection to 92 ppm (mean = 49 ppm, Fig. 8c) but do not show systematic stratigraphic behavior (Fig. 11b).

5. DISCUSSION

A number of studies have now demonstrated that Precambrian whole-rock, micrite and dolomicrite samples can yield interpretable CAS isotopic data in the absence of skeletal grains (e.g., Hurtgen et al., 2002, 2004; Zhang et al., 2003; Varni et al., 2001; Kaufman et al., 2002; Kah et al., 2004). In particular, the efforts of Kah et al. (2001, 2004) focused on the ~1.2 Ga Society Cliffs Formation, Bylot Supergroup, northern Baffin and Bylot islands, northeastern Canada, have helped validate the Precambrian relevance of the CAS method—even for dolomite—through a comparison of isotope data generated from interbedded carbonates and evaporites. But more important than the close isotope match between the meter-scale interbeds, the collective gypsum-CAS data set documents systematic and rapid isotopic changes of up to 20‰ over only a few hundred meters of stratigraphic section, which Kah et al. (2001, 2004) attributed to changes within the global ocean. Their arguments for global controls, explored within the context of the present study, are developed in the discussion that follows.

Kah et al. (2004) estimated that the roughly 20‰ isotopic variability recorded in the Society Cliffs Formation spans only several million years, whereas $\delta^{34}S$ shifts of similar magnitude define the first-order isotopic trends recorded in the Phanerozoic over much longer (10^7-to-10^8 year) time scales (Claypool et al., 1980; Kampschulte and Strauss, 2004). The possibility of comparatively rapid S isotope variability in the world ocean led Kah et al. (2004) to propose lower sulfate concentrations in Proterozoic seawater. The rate of S isotope change is inversely related to the amount of sulfate in the ocean and positively correlated with input/output terms that control selective removal or addition of ^{32}S in the ocean (Kump, 1989). In other words, the rate of change is inversely proportional to the residence time of sulfate in the ocean. Variations in flux terms could be related, for example, to (1) the widespread oxygen deficiency and possible euxinia hypothesized for the mid-Proterozoic ocean (Canfield, 1998; Anbar and Knoll, 2002; Arnold et al., 2004; Poulton et al., 2004) and the concomitantly efficient burial of pyrite attributable to the anoxia (Lyons and Berner, 1992; Hurtgen et al., 2005), as well as the general absence of bioturbation during the Proterozoic; (2) varying weathering controls, as perhaps linked to atmospheric pO_2 and pCO_2 or continental tectonics; and (3) tectonic controls on sulfur cycling (e.g., the seafloor spreading model of Carpenter and Lohmann, 1997; see Canfield, 2005).

Kah et al. (2004) specifically estimated the rate of isotopic change ($d\delta^{34}S/dt$) for the carbonates of the Society Cliffs Formation and, using this estimate and a simple mass balance approach modified from Kump and Arthur (1999), calculated the concentration of sulfate in the Mesoproterozoic ocean. Kah et al. (2004) applied the same approach to the data now available in this paper (Figs. 10a and 11a) for the Helena and Paradise Creek formations, as well as the ~1.3 Ga Dismal Lakes Group in northwestern Canada. Assuming deposition rates of 30 and 50 m/Myr (meters/million years)—choices they justify—Kah et al. calculated $d\delta^{34}S/dt$ values of 2.3 and 3.8‰/Myr and 6.0 and 10.0‰/Myr for the Helena and Paradise Creek, respectively. These rates of isotopic change yielded estimates of sulfate concentration of 2.4 and 1.5 mM and 0.9 and 0.5 mM, respectively. By contrast, the modern seawater concentration of 28–29 mM buffers the sulfate-S isotope system against changes at rates greater than 0.5‰/Myr. Kah et al. (2004) modeled additional data and suggested a progressive increase in seawater sulfate concentration through the Proterozoic—an increase they attributed to protracted biospheric oxygenation. Carbon isotope data spanning the Proterozoic suggest that the ocean-atmosphere increased in oxygen concentration progressively and perhaps incrementally as a result of the burial of reduced carbon (Des Marais et al., 1992; Des Marais, 1997; Frank et al., 2003; Bartley and Kah, 2004), thus providing a

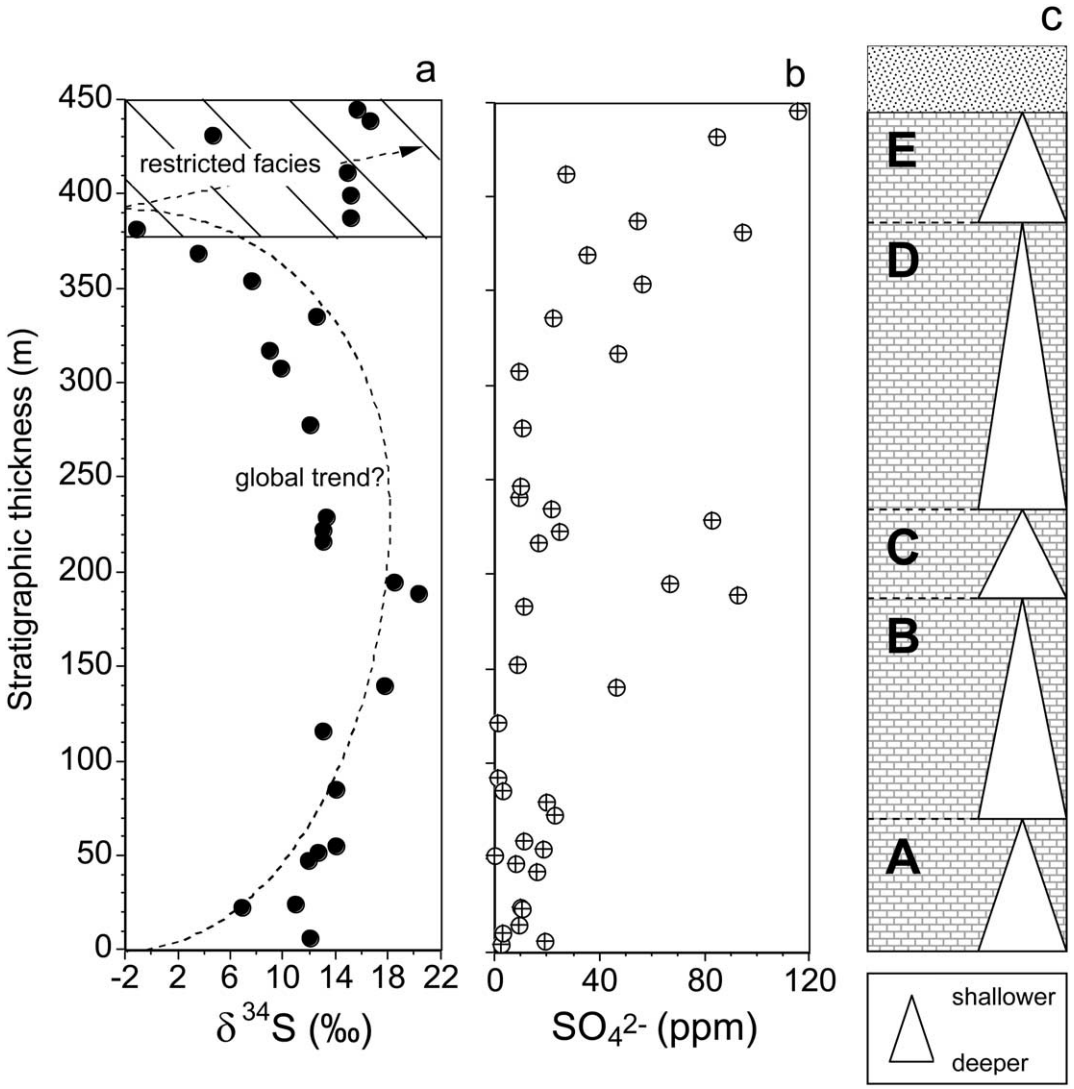

Fig. 10. Ousel Creek section of the Helena Formation, Belt Supergroup, Montana: (a) sulfur isotope compositions ($\delta^{34}S_{CAS}$) and (b) CAS concentrations (ppm sulfate). The section (c) is dominantly limestone comprising five shallowing-upward cycles (A-E) culminating ultimately with the sandy base of the overlying Missoula group. The basal cycle A contains abundant *Baicalia* and *Conophyton* stromatolites that define a marker zone that spans much of the Belt basin. Although the carbonates of the entire section show abundant lithologic variability in the context of the defined cycles, including intraclastic intervals, dolomitic zones, and stromatolites, the uppermost cycle (E) shows the most extreme signs of persistent shallowing and likely basin restriction. This interval is dominated by desiccation cracks; oolitic beds; cross-bedded grainstones; and intraclastic layers, including flat pebble conglomerates.

mechanism for a mid-to-late-Proterozoic increase in the amount of seawater sulfate.

CAS isotopic results for the Helena Formation suggest a systematic, up-section $\delta^{34}S$ increase followed by a decrease of ~20‰ spanning the lower 380 m of section (Fig. 10a). CAS concentrations are relatively low and invariant over this interval, with the exception of an increase roughly coincident with the heaviest $\delta^{34}S$ values at ~200 m. The uppermost portion of the Helena section shows a pronounced increase in $\delta^{34}S_{CAS}$. This abrupt ^{34}S enrichment corresponds with the occurrence of desiccation features and other sedimentological indicators of shallow and likely restricted deposition. This transition occurs in concert with an increase in CAS concentration (beginning at or just below ~380 m), suggesting increasing salinity and perhaps local controls on the S isotope composition of sulfate. For example, pyrite burial in combination with net evaporation in a setting with a limited marine connection would drive up both the CAS concentration and its $\delta^{34}S$ value. Beyond the local lithologic indicators of restriction for the upper part of the analyzed section, the associated facies change overlies several shallowing-upward cycles that culminate with the onset of subaerial exposure and basin restriction. The subaerial exposure is represented ultimately by a transition into the terrigenous facies of the overlying Snowslip Formation (Winston and Link, 1993; Winston and Lyons, 1997). More importantly, the observed relationship between CAS concentration and independent lithofacies proxies for restricted deposition suggests preservation of primary trends for CAS concentration, if not

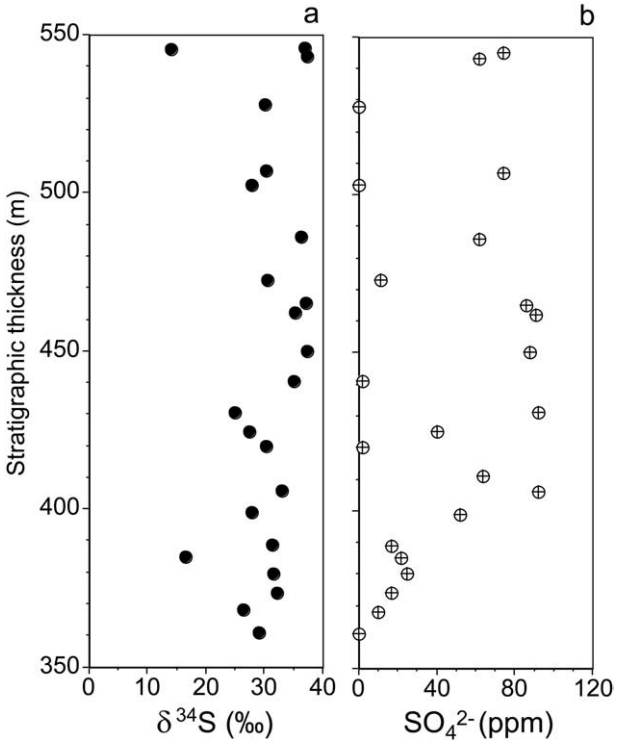

Fig. 11. Oxide Creek section of the Paradise Creek Formation, McNamara Group, northwest Queensland: (a) sulfur isotope compositions ($\delta^{34}S_{CAS}$) and (b) CAS concentrations (ppm sulfate). With the exception of the stromatolitic intervals, the dolostones that dominate the section are relatively uniform throughout (see text for details).

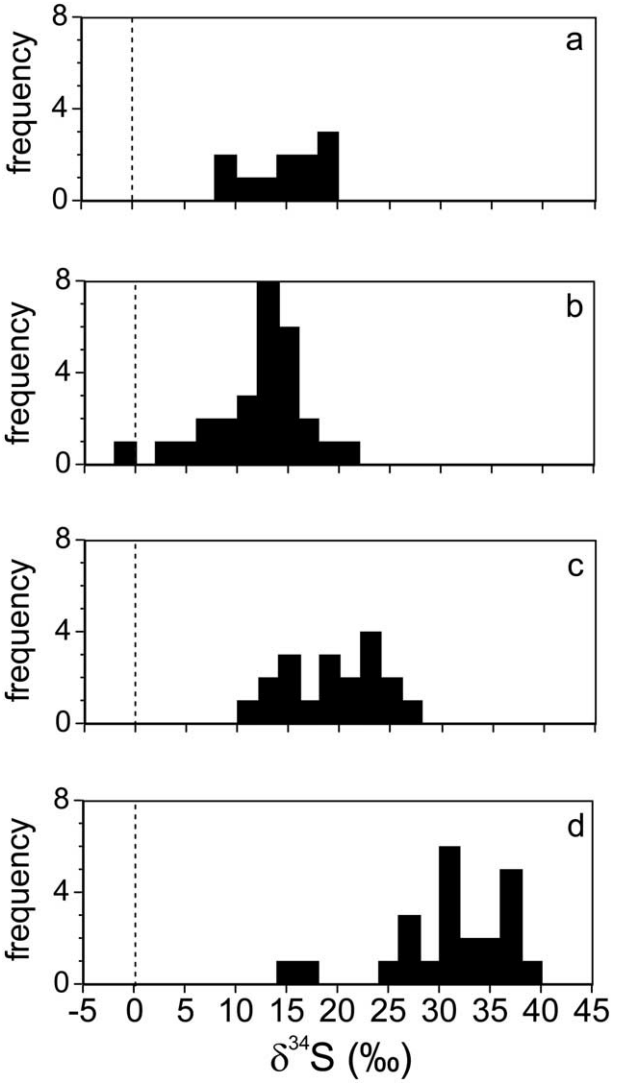

Fig. 12. Sulfur isotope compositions of (a) Mescal Limestone, Apache Group, central Arizona; (b) Helena Formation, Belt Supergroup, Montana; (c) Newland Formation, Belt Supergroup, Montana; and (d) Paradise Creek Formation, McNamara Group, northwest Queensland.

absolute values, despite potential losses during diagenesis. Kah et al. (2004) described similar continuity between CAS concentrations and facies evidence for restriction and corresponding elevated salinities in carbonates of the Society Cliffs Formation.

If the trend for $\delta^{34}S$ in the lower ~380 m of the Helena section is recording a global rather than local signal, the question remains whether the concentration spike centered at ~200 m also records ocean-scale controls (Fig. 10b). Furthermore, it is unlikely that sulfate in the global ocean shifted to negative $\delta^{34}S$ values, as is observed (–1.1‰) at the uppermost limit of this trend. Nevertheless, the comparatively systematic, and potentially global, portion of the Helena CAS curve is analogous in magnitude and stratigraphic thickness to S isotope shifts reported for pyrite and pyrrhotite from the Newland and Prichard formations of the lower Belt Supergroup (Fig. 4; Luepke and Lyons, 2001). Similarly, sulfide and sulfate isotope data for the Belt and the stratigraphic trend reported for the gypsum and CAS of the Bylot Supergroup are generally similar in their styles of isotopic variability (Kah et al., 2001, 2004).

Lyons et al. (2000) used $\delta^{34}S_{pyrite}$ data from unmetamorphosed organic-rich shales of the Newland Formation (−8.7‰ to +36.3‰; mean = +7.6‰, n = 41) to argue for episodic inputs of marine sulfate into a restricted (rift) setting. Stratigraphic trends were interpreted to reflect temporal variation in the integrity of the local marine connection, with S isotope shifts tracking the extent of reservoir isolation. According to this model, the highest $\delta^{34}S_{pyrite}$ value reflects the most extreme basin restriction. Many of the pyrite results fall within the same range as the limited number of available $\delta^{34}S_{barite}$ data of roughly the same age (+13.3‰ to +18.3‰, Zieg and Leitch, 1998; Strauss and Schieber, 1990; Lyons et al., 2000; Luepke and Lyons, 2001) and the $\delta^{34}S_{CAS}$ results from limestones in the Newland Formation (Fig. 12c, this study). This overlap is consistent with overall limitations in sulfate availability on local or global scales. Luepke and Lyons (2001) reported analogous stratigraphic S isotope trends ($\delta^{34}S$ variability of tens of per mil over 10^2 m stratigraphic thickness) for pyrite and pyrrhotite in the Belt basin west of the Helena Embayment. As in Lyons et al. (2000), Luepke and Lyons (2001) attributed pronounced ^{34}S enrichments and stratigraphic trends for the lower Belt sulfide to a tenuous and temporally varying connection between the Belt basin and the world ocean. At that time, however, they considered it likely that the predominance of

^{34}S-enriched pyrite and pyrrhotite in Belt sediments was also linked to low sulfate availability in the Proterozoic ocean.

The comparatively rapid isotopic variability that characterizes the bacteriogenic pyrite of the Belt Supergroup, and the pyrrhotite that derives from its metamorphism, is a style of $\delta^{34}S$ variability now recognized in many Proterozoic sulfides (e.g., Ross et al., 1995; Strauss, 1997, 2002), including sedimentary exhalative (SEDEX) sulfide deposits (Carr and Smith, 1977; Smith et al., 1978; Lyons et al., 2005). The general coherence of the isotopic trends among a number of mid-Proterozoic sections of widely different geographic position, geologic age, and depositional setting, and recorded in both sulfate and sulfide data, suggests a style of isotope behavior that is more likely a product of global oceanic trends than local processes. Admittedly, restricted basinal settings are not uncommon in the Proterozoic, but recognition of the isotopic pattern in settings such as the Society Cliffs Formation strengthens the ocean-scale hypothesis. Independent geochemical arguments can be made for a marine origin of Society Cliffs gypsum, with well preserved seawater signals (Kah et al., 2001). Therefore, in contrast to earlier arguments for changing local reservoir conditions to explain the observed large magnitude S isotope shifts over comparatively thin stratigraphic intervals in lower Belt sulfides (Lyons et al., 2000; Luepke and Lyons, 2001), both CAS and iron sulfide data from the Belt Supergroup may be dominated by the isotopic trends of the global ocean (also Lyons et al., 2004b). The iron sulfide data of the Belt, and likely other Proterozoic units, track the sulfate isotopic trend of the ocean because of overall limited sulfate availability due to the restricted depositional settings in combination with lower sulfate within the world ocean.

We do not mean to imply temporal equivalence for any of these isotopic records, but rather a similar pattern of isotopic variability defined only by large isotopic shifts over comparatively short stratigraphic intervals. Also, the observation that $\delta^{34}S$ values both increase and decrease in the sulfate and sulfide data suggests that the common thread is not simply progressive isotopic evolution through bacterial sulfate reduction and pyrite burial within individual restricted marine rift basins (Lyons et al., 2005). $\delta^{34}S$ values in such settings would consistently increase up-section. Finally, CAS results from the Helena and Newland formations corroborate the sulfide-based arguments of Lyons et al. (2000) and Luepke and Lyons (2001) for marine inputs to the Belt basin.

The $\delta^{34}S_{CAS}$ results for the Mescal Limestone suggest a 10‰ up-section decrease followed by a similar increase over only ~30 m of total section (Fig. 9a). Using the model of Kah et al. (2004), the ~1.2 Ga Mescal isotopic data would yield a sulfate concentration even lower than the 0.5 to 0.9 mM estimate of Kah et al. for the ~1.65 Ga carbonates of the Paradise Creek Formation based on data from the present study. By contrast, estimates for the ~1.2 Ga Society Cliffs Formation were 2.7 to 4.5 mM. If the model of Kah et al. is correct, this disparity suggests that sulfate did not increase progressively in a simple way through the Proterozoic. Alternatively, any or all of the isotopic trends might be modified by local primary or secondary overprints.

The Paradise Creek Formation (Fig. 11a) shows large variability but lacks the distinct stratigraphic trends observed in the other mid-Proterozoic units. The reason for the more scattered distribution of $\delta^{34}S_{CAS}$ values is presently unknown but may reflect diagenetic alteration of primary signals or local basin controls that overprint the global ocean signal. Nevertheless, the large range of values over a comparatively thin interval is consistent with the low-sulfate ocean model, and Kah et al. (2004) were able to approximate seawater sulfate from the observed data. In fact, the seemingly noisier data of the Paradise Creek may be a fundamental product of very low levels of sulfate in the ocean.

The low sulfate concentrations in the mid-Proterozoic ocean inferred from the rapid isotopic reservoir response expressed in numerous sulfide and sulfate isotope data may also be recorded in the general scarcity of bedded gypsum before ~1.3 Ga. In addition to limited sulfate availability, calcium in the ocean may have been drawn down by abundant calcium carbonate precipitation under high degrees of supersaturation (Grotzinger, 1989; Grotzinger and Kasting, 1993), further elevating the degree of evaporation required to achieve gypsum saturation (Kah et al., 2001, 2004). Limited sulfate availability might also be expressed in the preponderance of ^{34}S-enriched mid-Proterozoic iron sulfides (Lambert and Donnelly, 1991; Bottomley et al., 1992; Logan et al., 1995; Canfield, 1998; Canfield and Raiswell, 1999; Gorjan et al., 2000; Shen et al., 2002, 2003; Strauss, 2002; Lyons et al., 2005). Furthermore, given that sulfate is argued to inhibit dolomite formation (Baker and Kastner, 1981), the great abundance of Precambrian dolomite might reflect limited sulfate availability in the ocean.

Although Kah et al. (2004) suggested an overall increase in seawater sulfate concentration throughout the Proterozoic, the low concentrations associated with the Neoproterozoic intervals of major glaciation could reflect general deficiencies in the Proterozoic ocean that were exacerbated by sulfate reduction within an isolated, anoxic ice-covered ocean and reduced riverine delivery stemming from the suppressed hydrologic cycle under extensive sea-ice cover (Hurtgen et al., 2002). In addition to low CAS concentrations (Hurtgen et al., 2002, 2004), Hurtgen et al. (2002) presented abrupt $\delta^{34}S_{CAS}$ shifts as a proxy for low sulfate in Neoproterozoic seawater.

All of the samples in the present study yielded low CAS concentrations, which are similar to those described by Hurtgen et al. (2002, 2004) for Proterozoic carbonates but are one to two orders of magnitude or more below those typical of the Phanerozoic. Modern weathering may be a factor, but significant variations in $\delta^{34}S_{CAS}$ and CAS concentrations do not occur between samples where all weathered surfaces were removed versus those in which the weathering of dolomite penetrated the entire sample through fractures. For example, Paradise Creek samples at 379.5 m and 528.0 m were highly weathered, yet neither their sulfur isotope compositions nor CAS concentrations deviate from those of nearby samples. Much work remains before the effects of diagenesis will be completely understood. Unanswered or partially answered questions include the impacts of subsurface brines and pore fluids that are isotopically evolved through bacterial sulfate reduction, primary mineralogical controls, the timing and quantitative significance of cementation and dolomitization and associated sulfate reservoirs, and the effects of abundant iron sulfide formation. In our experience, many of these concerns can be minimized by emphasizing, as we have here, samples of nearly pure, organic- and pyrite-deficient carbonate lithologies. Given the various

lines of supporting evidence, the isotopic patterns described here and, to some extent, the CAS concentration relationships appear to be tracking primary trends in the mid-Proterozoic ocean. This global interpretation is supported by the observation that trends expressed in the data of the present study, with the possible exception of the elevated CAS concentration at the top of the Helena section, appear to be independent of local lithofacies relationships, including pronounced isotopic variability observed across relatively uniform lithologic intervals.

Throughout this discussion we have emphasized the unique nature of $\delta^{34}S_{CAS}$ variability expressed in Proterozoic carbonate rocks and similar patterns observed in iron sulfides. These patterns of up to a few tens of permil variability are recorded over only tens to hundreds of meters of section, which may represent only a few million years or less. By contrast, 20‰ variability characterizes first-order variations spanning tens to hundreds of millions of years in the Phanerozoic (Claypool et al., 1980; Kampschulte and Strauss, 2004). Interestingly, the Phanerozoic curve of Kampschulte and Strauss (2004) shows significant $\delta^{34}S$ variability for evaporite and CAS data over substantially narrower intervals. These variable data are plotted as single ages in the compilation curves, and any shorter-term stratigraphic trends are consequently lost.

Recent CAS work by Gill et al. (2004) confirms that systematic, stratigraphic variation spanning as much as ~20‰ may be occurring over only million-year time scales well into the Paleozoic, suggesting that seawater sulfate concentrations had not yet come close to modern values. Ancient sulfate levels estimated from fluid inclusions in halite generally support this assertion, although a terminal Proterozoic sulfate high expressed in the inclusion data, if correct, suggests that the increase may not have been simple and progressive (Horita et al., 2002; Brennan et al., 2004). Beyond any straightforward relationship between increasing atmospheric oxygen content and the associated weathering flux of sulfate, Canfield (2005) suggested that once the deep ocean became oxygenated late in the Proterozoic, the flux of deep-marine pyrite burial decreased, thus reducing the amount of sedimentary sulfur lost from the Earth surface system through subduction. Over time, the diminution of this sink could have resulted in a progressive increase in the sulfate content of seawater sulfate through the early Phanerozoic.

High-resolution $\delta^{34}S$ data generated for the Mesozoic and Cenozoic (Paytan et al., 1998, 2004) also reveal systematic, short-term isotopic excursions. Clearly, there is a hierarchy of processes, couplings, and feedbacks expressed in the Phanerozoic sulfur isotope data, including shorter-term linkages between sulfur cycling and the $\delta^{34}S$ of the ocean that are superimposed on the longer-term controls reflected in the first-order trend of Claypool et al. (1980) and Kampschulte and Strauss (2004). Although the data are still sparse, such a hierarchical relationship is suggested for the Proterozoic (Fig. 12). However, the shorter-term $\delta^{34}S$ shifts of the later Phanerozoic recorded in the marine barite data of Paytan et al. (1998, 2004) are smaller (on the order of 5‰) and longer (roughly 5 to 10 Myr) compared to those of the Proterozoic and likely the Paleozoic. Finally, beyond differences in the sulfate reservoir size, variations in sulfur burial/weathering fluxes play a central role in dictating $\delta^{34}S$ trends in the ocean over geologic time. Seawater sulfate concentration merely defines the isotopic sensitivity of the marine sulfate reservoir to such changes.

6. CONCLUSIONS

Our trends for carbonate-associated sulfate from the Mescal Limestone, the Helena and Newland formations of the Belt Supergroup, and the Paradise Creek Formation show large magnitude isotopic variability over comparatively narrow stratigraphic intervals. These trends are analogous to patterns widely recognized in mid-Proterozoic sulfide and sulfate isotope data, which routinely display up to and exceeding 20‰ variation over only tens to hundreds of meters of section. Given the inferred high rates of accumulation for shallow platform carbonates and for fine-grained siliciclastics in rifted settings such as the Belt basin, we can assume the observed isotopic variability occurred over significantly more rapid time scales (10^6 years or less) compared to the sulfate isotopic shifts of similar $\delta^{34}S$ magnitude historically described for the Phanerozoic. Such rapid variability has been ascribed to lower sulfate availability in the mid-Proterozoic ocean, with concentrations that may have only been 5% to 15% of those present today. Sulfate deficiencies are also suggested by the paucity of bedded gypsum deposits and the small net fractionations suggested by the abundance of ^{34}S-enriched pyrite in Proterozoic sediments. However, a rapidly varying isotope composition for the marine sulfate reservoir makes precise determinations of fractionations difficult unless $\delta^{34}S$ values are known for truly coeval sulfate and sulfide. Absent such constraints, falsely large (and small) fractionations may be surmised, and hypotheses addressing $\Delta^{34}S$ ($\delta^{34}S_{sulfate} - \delta^{34}S_{pyrite}$) trends through time (e.g., Canfield and Teske, 1996) become nontrivial (Hurtgen et al. 2002, 2005; Lyons et al., 2004b).

Although likely compromised by diagenesis, CAS concentrations that are consistently below 100 ppm, compared to the thousands of ppm observed in modern carbonate sediments, also suggest lower mid-Proterozoic seawater sulfate concentrations. A smaller marine sulfate reservoir, which was largely a result of lower atmospheric oxygen levels, would have resulted in greater sensitivity to the controls on isotopic variability. Extensive bacterial sulfate reduction in a hypothesized anoxic mid-Proterozoic ocean and correspondingly efficient burial of S as pyrite could also limit sulfate concentrations. In the modern ocean, euxinic settings are seldom characterized by water-column sulfide concentrations in excess of 0.5–1.0 mM. Given this observation, it is important to consider whether euxinic environments in a lower-sulfate ocean may have contained less hydrogen sulfide than a Phanerozoic regional- or ocean-scale equivalent (Shen et al., 2002; Lyons et al., 2004b; Hurtgen et al., 2005) and what impact this might have had on trace-metal bioavailability (Anbar and Knoll, 2002).

Response times of isotopic systems are strongly influenced by their residence times in the ocean. Therefore, in the presence of lower sulfate concentrations, flux terms such as pyrite burial, sulfide and sulfate weathering, and seafloor volcanism can drive comparatively rapid $\delta^{34}S$ fluctuations in the global seawater sulfate reservoir. Widespread oxygen deficiency within the deep ocean would favor efficient pyrite burial, and weathering would be linked to variations in pO_2,

continental tectonics, and, during Neoproterozoic glaciations, possible perturbations of the hydrologic cycle. The role of seafloor tectonic/volcanic activity would, in part, reflect patterns of supercontinent formation and breakup. Lower-than-modern sulfate concentrations may have persisted into at least the early-to-middle portions of the Paleozoic, where comparatively rapid ocean-scale $\delta^{34}S$ variability is superimposed on the long-term, first-order trends that are well characterized in the literature. Evaporite deposits are limited throughout the geologic record, particularly the Precambrian, and inferring patterns of $\delta^{34}S$ variability for seawater sulfate based only on pyrite isotopic data can be challenging. Given these limitations, and because we know of few if any modern or ancient example where $\delta^{34}S_{CAS}$ values have been obviously modified in any appreciable way during diagenesis, the CAS results presented here and elsewhere have become an increasingly important window to the chemistry of the early ocean and atmosphere.

Acknowledgments—Financial support was provided by National Science Foundation grant EAR-9725538 (T.W.L.), the Belt Association (A.M.G.), and the University of Missouri Research Board. We thank Jon Fong, Steve Studley, Carol Nabelek, Linda Kah, Tracy Frank, Jim Luepke, and Peter Southgate for laboratory and field assistance and Mike Formolo for his insightful comments. We are particularly grateful to Don Winston for his generous help in the field, assistance with drill core collection, and for many stimulating discussions. Matt Hurtgen, Marty Goldhaber, and two anonymous reviewers provided invaluable reviews of this manuscript.

Associate editor: M. B. Goldhaber

REFERENCES

Aleinikoff J. N., Evans K. V., Fanning C. M., Obradovich J. D., Ruppel E. T., Zieg J. A., and Steinmetz J. C. (1996) SHRIMP U-Pb ages of felsic igneous rocks, Belt Supergroup, Western Montana. *Geol. Soc. Am. Abst. Prog.* **28,** A-376.

Anbar A. D. and Knoll A. H. (2002) Proterozoic ocean chemistry and evolution: A bioinorganic bridge. *Science* **297,** 1137–1142.

Anderson H. E. and Davis D. W. (1995) U-Pb geochronology of the Moyie sills, Purcell Supergroup, southeastern British Columbia: Implications for the Mesoproterozoic geological history of the Purcell (Belt) basin. *Can. J. Earth Sci.* **32,** 1180–1193.

Arnold G. L., Anbar A. D., Barling J., and Lyons T. W. (2004) Molybdenum isotope evidence for widespread anoxia in mid-Proterozoic oceans. *Science* **304,** 87–90.

Arthurton R. S. (1973) Experimentally produced halite compared with Triassic layered halite-rock from Cheshire, England. *Sedimentology* **20,** 145–160.

Baker P. A. and Kastner M. (1981) Constraints on the formation of sedimentary dolomite. *Science* **213,** 214–216.

Bartley J. K. and Kah L. C. (2004) Marine carbon reservoir, C_{org}–C_{carb} coupling and the evolution of the Proterozoic carbon cycle. *Geology* **32,** 129–132.

Beenus M. A. and Knauth L. P. (1985) Preserved stable isotopic signature of subaerial diagenesis in the 1.2 b.y. Mescal Limestone, central Arizona: Implications for the timing and development of a terrestrial plant cover. *Geol. Soc. Am. Bull.* **96,** 737–745.

Bekker A., Holland H. D., Wang P.-L., Rumble D. III, Stein H. J., Hannah J. L., Coetzee L. L., and Beukes N. J. (2004) Dating the rise of atmospheric oxygen. *Nature* **427,** 117–120.

Berner R. A. (1982) Burial of organic carbon and pyrite sulfur in the modern ocean, its geochemical and environmental significance. *Am. J. Sci.* **282,** 451–473.

Berner R. A. and Raiswell R. (1983) Burial of organic carbon and pyrite sulfur in sediments over Phanerozoic time: A new theory. *Geochim. Cosmochim. Acta* **47,** 855–862.

Bertrand-Sarfati J. and Awramik S. M. (1992) Stromatolites of the Mescal Limestone (Apache Group, Middle Proterozoic, central Arizona): Taxonomy, biostratigraphy and paleoenvironments. *Geol. Soc. Am. Bull.* **104,** 1138–1155.

Blake D. H. and Stewart A. J. (1992) Stratigraphic and tectonic framework, Mount Isa Inlier. In *Detailed Studies of the Mount Isa Inlier* (eds. A. J. Stewart and D. H. Blake), Bureau of Mineral Resources **243,** 1–11.

Bottomley D. J., Veizer J., Nielsen H., and Modczydlowska M. (1992) Isotopic composition of disseminated sulfur in Precambrian sedimentary rocks. *Geochim. Cosmochim. Acta* **56,** 3311–3322.

Brennan S. T., Lowenstein T. K., and Horita J. (2004) Seawater chemistry and the advent of biocalcification. *Geology* **32,** 473–476.

Burdett J. W., Arthur M. A., and Richardson M. (1989) A Neogene seawater isotope age curve from calcareous pelagic microfossils. *Earth Planet. Sci. Lett.* **94,** 189–198.

Busenberg E. and Plummer L. N. (1985) Kinetic and thermodynamic factors controlling the distribution of SO_4^{2-} and Na^+ in calcites and selected aragonites. *Geochim. Cosmochim. Acta* **49,** 713–725.

Canfield D. E. (1998) A new model for Proterozoic ocean chemistry. *Nature* **396,** 450–453.

Canfield D. E. (2001) Isotope fractionation by natural populations of sulfate-reducing bacteria. *Geochim. Cosmochim. Acta* **65,** 1117–1124.

Canfield D. E. (2005) The evolution of the Earth surface sulfur reservoir. *Am. J. Sci.* **304**, 839–861.

Canfield D. E. and Raiswell R. (1999) The evolution of the sulfur cycle. *Am. J. Sci.* **299,** 697–723.

Canfield D. E. and Teske A. (1996) Late Proterozoic rise in atmospheric oxygen concentration inferred from phylogenic and sulfur-isotope studies. *Nature* **382,** 127–132.

Canfield D. E. and Thamdrup B. (1994) The production of ^{34}S-depleted sulfide during bacterial disproportionation of elemental sulfur. *Science* **266,** 1973–1975.

Canfield D. E., Habicht K. S., and Thamdrup B. (2000) The Archean sulfur cycle and the early history of atmospheric oxygen. *Science* **288,** 658–661.

Carpenter S. J. and Lohmann K. C. (1997) Carbon isotope ratios of Phanerozoic marine cements: Re-evaluating the global carbon and sulfur systems. *Geochim. Cosmochim. Acta* **61,** 4831–4846.

Carr G. R. and Smith J. W. (1977) A comparative isotopic study of the Lady Loretta zinc-lead-silver deposit. *Mineral. Deposita* **12,** 105–110.

Chambers L. A. and Trudinger P. A. (1979) Microbiological fractionation of stable sulfur isotopes: A review and critique. *Geomicrobiol. J.* **1,** 249–293.

Chambers L. A., Trudinger P. A., Smith J. W., and Burns M. S. (1975) Fractionation of sulfur isotopes by continuous cultures of *Desulfovibrio desulfuricans. Can. J. Microbiol.* **21,** 1602–1607.

Claypool G., Holser W. T., Kaplan I. R., Sakai H., and Zak I. (1980) The age curves of sulfur and oxygen isotopes in marine sulfate and their mutual interpretation. *Chem. Geol.* **28,** 199–260.

Cressman E. R. (1989) Reconnaissance stratigraphy of the Prichard Formation (Middle Proterozoic) after development of the Belt basin, Washington, Idaho and Montana. USGS Prof. Paper 1490.

Damon P. E., Livingston D. E., and Erickson R. C. (1962) New K-Ar dates for the Precambrian of Pinal, Gila, Yavapai and Coconino Counties, Arizona. In *Mogollon Rim Region, East Central Arizona* (eds. Weber and R. H. Pierce) H. W., *New Mexico Geol. Soc. Guidebook, 13th Field Conference,* 56–57.

Des Marais D. J. (1997) Isotopic evolution of the biogeochemical carbon cycle during the Proterozoic Eon. *Org. Geochem.* **27,** 185–193.

Des Marais D. J., Strauss H., Summons R. E., and Hayes J. M. (1992) Carbon isotope evidence for the stepwise oxidation of the Proterozoic atmosphere. *Nature* **359,** 605–609.

Detmers J., Brüchert V., Habicht K. S., and Kuever J. (2001) Diversity of sulfur isotope fractionations by sulfate-reducing prokaryotes. *Appl. Environ. Microbiol.* **67,** 888–894.

Farquhar J. and Wing B. A. (2003) Multiple sulfur isotopes and the evolution of the atmosphere. *Earth Planet. Sci. Lett.* **213,** 1–13.

Farquhar J., Bao H., and Thiemens M. (2000) Atmospheric influence of Earth's earliest sulfur cycle. *Science* **289,** 756–758.

Fletcher K. E., Heizler M. T., Karlstrom K. E., Timmons J. M., Crossey L. J., and Block J. D. (2004) Provenance and geochronology of Mesoproterozoic sedimentary rocks from across the southwest United States revealed in $^{40}Ar/^{39}Ar$ dating of detrital muscovites. *Geol. Soc. Am. Abst. Prog.* **36,** 405.

Frank T. D., Kah L. C., and Lyons T. W. (2003) Changes in organic matter production and accumulation as a mechanism for isotopic evolution in the Mesoproterozoic ocean. *Geol. Mag.* **140,** 397–420.

Gill B. C., Lyons T. W., and Saltzman M. R. (2004) Parallel high-resolution carbon and sulfur isotope records in the Paleozoic and implications for biospheric oxygenation. *Geol. Soc. Am. Abst. Prog.* **36,** 477.

Gorjan P., Veevers J. J., and Walter M. R. (2000) Neoproterozoic sulfur-isotope variation in Australia and global implications. *Precambrian Res.* **100,** 151–179.

Grotzinger J. P. (1989) Facies and evolution of Precambrian carbonate depositional systems: Emergence of the modern platform archetype. In *Controls on Carbonate Platform and Basin Development* (eds. P. D. Crevello, J. L. Wilson, J. F. Sarg, and J. F. Read). *SEPM Spec. Pub.* **44**, 79–101.

Grotzinger J. P. and Kasting J. F. (1993) New constraints on Precambrian ocean composition. *J. Geol.* **101,** 235–258.

Habicht K. S. and Canfield D. E. (1996) Sulphur isotope fractionation in modern microbial mats and the evolution of the sulphur cycle. *Nature* **382,** 342–343.

Habicht K. S. and Canfield D. E. (1997) Sulfur isotope fractionation during bacterial sulfate reduction in organic-rich sediments. *Geochim. Cosmochim. Acta* **61,** 5351–5361.

Habicht K. S. and Canfield D. E. (2001) Isotope fractionation by sulfate-reducing natural populations and the isotopic composition of sulfide in marine sediments. *Geology* **29,** 555–558.

Habicht K. S., Canfield D. E., and Rethmeier J. (1998) Sulfur isotope fractionation during bacterial reduction and disproportionation of thiosulfate and sulfite. *Geochim. Cosmochim. Acta* **62,** 2585–2595.

Habicht K. S., Gade M., Thamdrup B., Berg P., and Canfield D. (2002) Calibration of sulfate levels in the Archean Ocean. *Science* **298,** 2372–2374.

Harrison A. G. and Thode H. G. (1958) Mechanism of the bacterial sulfate reduction of sulphate from isotope fractionation studies. *Trans. Faraday Soc.* **54,** 84–92.

Harrison J. E. (1972) Precambrian Belt basin of northwestern United States—Its geometry, sedimentation and copper occurrences. *Geol. Soc. Am. Bull.* **83,** 1215–1240.

Harrison J. E., Griggs A. B., and Wells J. D. (1974) Tectonic features of the Precambrian Belt basin and their influence on post-Belt structures. USGS Prof. Paper 866.

Holland H. D. (1999) Early life on Earth. *Geochem. News* **100,** 2019.

Holland H. D. (2002) Volcanic gases, black smokers and the Great Oxidation Event. *Geochim. Cosmochim. Acta* **66,** 3811–3826.

Holser W. T. and Kaplan I. R. (1966) Isotope geochemistry of sedimentary sulfates. *Chem. Geol.* **1,** 93–135.

Horita J., Zimmermann H., and Holland H. D. (2002) Chemical evolution of seawater during the Phanerozoic: Implications from the record of marine evaporites. *Geochim. Cosmochim. Acta* **66,** 3733–3756.

Hurtgen M. T., Arthur M. A., and Halverson G. P. (2005) Neoproterozoic S isotopes, the evolution of microbial S species and the burial efficiency of sulfide as sedimentary pyrite. *Geology* **33,** 41–44.

Hurtgen M. T., Arthur M. A., and Prave A. R. (2004) The sulfur isotope composition of carbonate-associated sulfate in Mesoproterozoic to Neoproterozoic carbonates from Death Valley, California. In *Sulfur Biogeochemistry—Past and Present* (eds. J. P. Amend, K. J. Edwards, and T. W. Lyons). *Geol. Soc. Am. Spec. Paper* **379,** 177–194.

Hurtgen M. T., Arthur M. A., Suits N. S., and Kaufman A. J. (2002) The sulfur isotopic composition of Neoproterozoic seawater sulfate: Implications for a snowball Earth? *Earth Planet. Sci. Lett.* **203,** 413–429.

Indurm M. (2000) Toward a high resolution Late Palaeoproterozoic-earliest Mesoproterozoic apparent polar wander path for Northern Australia. *Aust. J. Earth Sci.* **47,** 405–429.

Kah L. C., Lyons T. W., and Chesley J. T. (2001) Geochemistry of a 1.2 carbonate-evaporite Succession, Northern Baffin Islands: Implications for Mesoproterozoic Marine Evolution. *Precambrian Res.* **111,** 203–234.

Kah L. C., Lyons T. W., and Frank T. D. (2004) Low marine sulphate and protracted oxygenation of the Proterozoic biosphere. *Nature* **431,** 834–838.

Kakegawa T., Hajime K., and Ohmoto H. (1998) Origins of pyrites in the approximately 2.5 Ga Mt. McRae Shale, the Hamersley District, Western Australia. *Geochim. Cosmochim. Acta* **62,** 3205–3220.

Kampschulte A. and Strauss H. (2004) The sulfur isotopic evolution of Phanerozoic seawater based on the analysis of structurally substituted sulfate in carbonates. *Chem. Geol.* **204,** 255–286.

Kampschulte A., Bruckschen P., and Strauss H. (2001) The sulphur isotopic composition of trace sulphates in Carboniferous brachiopods: Implication for coeval seawater, correlation with other geochemical cycles and isotope stratigraphy. *Chem. Geol.* **175,** 149–173.

Kaplan I. R. and Rittenberg S. C. (1964) Microbiological fractionation of sulphur isotopes. *J. Gen. Microbiol.* **34,** 195–212.

Kaufman A. J., Varni M. A., and Wing B. A. (2002) Sulfur isotope constraints on a Snowball Earth. *Geol. Soc. Am. Abst. Prog.* **34,** 221.

Kemp A. L. W. and Thode H. G. (1968) The mechanism of the bacterial reduction of sulphate and sulphite from isotope fractionation studies. *Geochim. Cosmochim. Acta* **32,** 71–91.

Kump L. R. (1989) Alternative modeling approaches to the geochemical cycles of carbon, sulfur and strontium isotopes. *Am. J. Sci.* **289,** 390–410.

Kump L. R. and Arthur M. A. (1999) Interpreting carbon-isotope excursions: Carbonates and organic matter. *Chem. Geol.* **161,** 181–198.

Lambert I. B. and Donnelly T. H. (1991) Atmospheric oxygen levels in the Precambrian: A review of isotopic and geological evidence. *Palaeogeog. Palaeoclimat. Palaeoecol.* **97,** 83–91.

Lasaga A. C. and Ohmoto H. (2002) The oxygen geochemical cycle: Dynamics and stability. *Geochim. Cosmochim. Acta* **66,** 361–381.

Logan G. A., Hayes J. M., Hieshima G. B., and Summons R. E. (1995) Terminal Proterozoic reorganization of biogeochemical cycles. *Nature* **376,** 53–56.

Longinelli A. (1989) Oxygen-18 and sulphur-34 in dissolved oceanic sulphate and phosphate. In *Handbook of Environmental Isotope Geochemistry,* Vol. 3 (eds. P. Fritz and J. FontesCh.), pp. 219–255. Elsevier.

Luepke J. J. and Lyons T. W. (2001) Pre-Rodinian (Mesoproterozoic) Supercontinental rifting along the western margin of Laurentia: Evidence from the Belt-Purcell Supergroup. *Precambrian Res.* **111,** 79–90.

Lyons T. W. and Berner R. A. (1992) Carbon-sulfur-iron systematics of the uppermost deep-water sediments of the Black Sea. *Chem. Geol.* **99,** 1–27.

Lyons T. W., Gellatly A. M., McGoldrick P. J., and Kah L. C. (2005) Proterozoic sedimentary exhalative (SEDEX) deposits and their links to evolving global ocean chemistry. In *Evolution of the Early Atmosphere, Hydrosphere and Biosphere: Constraints from Ore Deposits* (eds. H. Ohmoto and S. E. Kesler), *Geol. Soc. Am. Spec. Paper* (in press).

Lyons T. W., Gill B. C., Shim M.-J., Frank T. D., Hurtgen M. T., Saltzman M. R., Gellatly A. M., and Kah L. C. (2004a) Carbonate-associated sulfate as a paleoceanographic proxy: An update. 14th V. M. Goldschmidt Conference Abstracts. *Geochim. Cosmochim. Acta* **68** (**Suppl.**), A337.

Lyons T. W., Kah L. C., and Gellatly A. M. (2004b) The Precambrian sulphur isotope record of evolving atmospheric oxygen. In *The Precambrian Earth: Tempos and Events* (eds. P. G. Eriksson, W. Altermann, D. R. Nelson, W. U. Mueller, and O. Catuneanu). *Developments in Precambrian Geology* **12,** 421–440. Elsevier.

Lyons T. W., Walter L. M., Gellatly A. M., Martini A. M., and Blake R. E. (2004c) Sites of anomalous organic remineralization in the carbonate sediment of South Florida, USA: The sulfur cycle and carbonate-associated sulfate. In *Sulfur Biogeochemistry—Past and Present* (eds. J. P. Amend, K. J. Edwards, and T. W. Lyons). *Geol. Soc. Am. Spec. Paper* **379**, 161–176.

Lyons T. W., Luepke J. J., Schreiber M. E., and Zieg G. A. (2000) Sulfur geochemical constraints on Mesoproterozoic Restricted Ma-

rine Deposition: Lower Belt Supergroup, Northwest United States. *Geochim. Cosmochim. Acta* **64,** 427–437.

Maxwell D. T. and Hower J. (1967) High-grade diagenesis and low-grade metamorphism of illite in the Precambrian Belt Series. *Amer. Mineral.* **52,** 843–857.

Ohmoto H. and Felder R. P. (1987) Bacterial activity in the warmer, sulphate-bearing, Archaean oceans. *Nature* **328,** 244–246.

Ohmoto H., Kakegawa T., and Lowe D. R. (1993) 3.4-billion-year-old biogenic pyrites from Barberton, South Africa: Sulfur isotope evidence. *Science* **262,** 555–557.

Page R. W. and Sweet I. P. (1998) Geochronology of basin phases in the western Mt. Isa Inlier and correlation with the McArthur Basin. *Aust. J. Earth Sci.* **45,** 219–232.

Page R. W., Jackson M. J., and Krassay A. A. (2000) Constraining sequence stratigraphy of the Proterozoic Mt. Isa terrain. *Aust. J. Earth Sci.* **47,** 431–459.

Pavlov A. A., Hurtgen M. T., Kasting J. F., and Arthur M. A. (2003) Methane-rich Proterozoic atmosphere? *Geology* **31,** 87–90.

Paytan A., Kastner M., Campbell D. A., and Thiemans M. H. (1998) Sulfur isotopic composition of Cenozoic seawater sulfate. *Science* **282,** 1459–1462.

Paytan A., Kastner M., Campbell D., and Thiemens M. H. (2004) Seawater sulfur isotope fluctuations in the Cretaceous. *Science* **304,** 1663–1665.

Poulton S. W., Fralick P. W., and Canfield D. E. (2004) The transition to a sulphidic ocean ~1.84 billion years ago. *Nature* **431,** 173–177.

Rees C. E., Jenkins W. J., and Monster J. (1978) The sulfur isotopic composition of ocean water sulphate. *Geochim. Cosmochim. Acta* **42,** 377–381.

Ross G. M., Bloch J. D., and Krouse H. R. (1995) Neoproterozoic strata of the southern Canadian Cordillera and the isotopic evolution of seawater sulfate. *Precambrian Res.* **73,** 71–99.

Saltzman M. R., Brasier M. D., Ripperdan R. L., Ergaliev G. K., Lohmann K. C., Robison R. A., Chang W. T., Peng S., and Runnegar B. (2000) A global carbon isotope excursion during the Late Cambrian: Relation to trilobite extinctions, organic-matter burial and sea level. *Palaeogeog. Palaeoclimat. Palaeoecol.* **162,** 211–223.

Sami T. T., James N. P., Kyser T. K., Southgate P. N., Jackson M., and Page R. W. (2000) Evolution of late Proterozoic ramp systems, lower McNamara Group, northeastern Australia. In *Carbonate Sedimentation and Diagenesis in the Evolving Precambrian World* (eds. J. P. Grotzinger and N. P. James). *SEPM Spec. Pub.* **67,** 243–274.

Schidlowski M. (1983) Evolution of photoautotrophy and early atmospheric oxygen levels. In *Development and Interactions of the Precambrian Atmosphere, Lithosphere and Biosphere*: *Results and Challenges* (eds. B. Nagy, R. Weber, J. C. Guerrero, and M. Schidlowski). *Precamb. Res.* **20,** 319–335.

Sears J. W., Chamberlain K. R., and Buckley S. N. (1998) Structural and U-Pb geochronological evidence for 1.47 Ga rifting in the Belt basin, western Montana. *Can. J. Earth Sci.* **35,** 467–475.

Shen Y., Buick R., and Canfield D. E. (2001) Isotopic evidence for microbial sulphate reduction in the early Archaean era. *Nature* **410,** 77–81.

Shen Y., Canfield D. E., and Knoll A. H. (2002) Middle Proterozoic ocean chemistry: Evidence from the McArthur Basin, northern Australia. *Am. J. Sci.* **302,** 81–109.

Shen Y., Knoll A. H., and Walter M. R. (2003) Evidence for low sulphate and anoxia in a mid-Proterozoic marine basin. *Nature* **423,** 632–635.

Shim M.-J. (2004) Techniques for the analysis of carbonate-associated sulfate (CAS) concentrations in modern and ancient limestones and dolostones. M.S. thesis, University of Missouri-Columbia.

Shride A. F. (1967) Younger Precambrian geology in southern Arizona. USGS Prof. Paper 566.

Silver L. T. (1960) Age determinations on Precambrian diabase differentiates in the Sierra Ancha, Gila County, Arizona. *Geol. Soc. Am. Bull.* **71,** 1973–1974.

Silver L. T. (1978) Precambrian formations and Precambrian history in Cochise County, southeastern Arizona. In *Land of Cochise, Southeastern Arizona* (eds. J. F. Callender, J. C. Wilt, and R. E. Clemons). *New Mexico Geol. Soc. Guidebook, 29th Field Conference* 157–163.

Smith J. W., Burns M. S., and Croxford N. J. W. (1978) Stable isotope studies of the origins of mineralization at Mount Isa. I. *Mineral. Deposita* **13,** 369–381.

Southgate P. N., Scott D. L., Sami T. T., Domagala J., Jackson M. J., James N. P., and Kyser T. K. (2000) Basin shape and sediment architecture in the Gun Supersequence: A strike-slip model for Pb-Zn-Ag ore genesis at Mt. Isa. *Aust. J. Earth Sci.* **47,** 509–531.

Staudt W. J. and Schoonen M. A. A. (1995) Sulfate incorporation into sedimentary carbonates. In *Geochemical Transformations of Sedimentary Sulfur* (eds. M. A. Vairavamurthy and M. A. A. Schoonen), pp. 332–345. American Chemical Society.

Stewart J. H., Gehrels G. E., Barth A. P., Link P. K., Christie-Blick N., and Wrucke C. T. (2001) Detrital zircon provenance of Mesoproterozoic to Cambrian arenites in the western United States and northwest Mexico. *Geol. Soc. Am. Bull.* **113,** 1343–1356.

Strauss H. (1993) The sulfur isotopic record of Precambrian sulfates: New data and a critical evaluation of the existing record. *Precambrian Res.* **63,** 225–246.

Strauss H. (1997) The isotopic composition of sedimentary sulfur through time. *Palaeogeog. Palaeoclimat. Palaeoecol.* **132,** 97–118.

Strauss H. (1999) Geological evolution from isotope proxy signals–sulfur. *Chem. Geol.* **161,** 89–101.

Strauss H. (2002) The isotopic composition of Precambrian sulphides—Seawater chemistry and biological evolution. In *Precambrian Sedimentary Environments: A Modern Approach to Ancient Depositional Systems* (eds. W. Altermann and P. L. Corocoran). *Int. Assoc. Sediment. Spec. Pub.* **33,** 67–105.

Strauss H. and Schieber J. (1990) A sulfur isotopic study of pyrite genesis: The mid-Proterozoic Newland Formation, Belt Supergroup, Montana. *Geochim. Cosmochim. Acta* **54,** 197–204.

Strauss H., Banerjee D. M., and Kumar V. (2001) The sulfur isotopic composition of Neoproterozoic to early Cambrian seawater-evidence from the cyclic Hanseran evaporites, NW India. *Chem. Geol.* **175,** 17–28.

Takano B. (1985) Geochemical implications of sulfate in sedimentary carbonates. *Chem. Geol.* **49,** 393–403.

Varni M. A., Kaufman A. J., Misi A., and Brito Neves B. B. (2001) Anomalous $\delta^{34}S$ signatures in trace sulfate potential cap carbonate in the Neoproterozoic Bambui Group, Brazil. *Geol. Soc. Am. Abst. Prog.* **33,** A-95.

Veizer J., Ala D., Azmy K., Bruckschen P., Buhl D., Bruhn F., Cardon G. A. F., Diener A., Ebneth S., Godderis Y., Jasper T., Korte C., Pawallek F., Podlaha O. G., and Strauss H. (1999) $^{87}Sr/^{86}Sr$, $\delta^{13}C$ and $\delta^{18}O$ evolution of Phanerozoic seawater. *Chem. Geol.* **161,** 59–88.

Walter L. M. and Burton E. A. (1990) Dissolution of recent platform carbonate sediments in marine pore fluids. *Am. J. Sci.* **290,** 601–643.

Walter L. M., Bischof S. A., Patterson W. P., and Lyons T. W. (1993) Dissolution and recrystallization in modern shelf carbonates: Evidence from pore water and solid phase chemistry. *Phil. Trans. Royal Soc. London A* **344,** 27–36.

Winston D. (1990) Evidence for intracratonic, fluvial and lacustrine settings of Middle and Late Proterozoic basins of western USA. In *Mid-Proterozoic Laurentia-Baltica* (eds. C. F. Gower, T. Rivers, and B. Ryan). *Geol. Assoc. Canada Spec. Paper* **38,** 535–564.

Winston D. and Link P. K. (1993) Middle Proterozoic rocks of Montana, Idaho and eastern Washington: The Belt Supergroup Precambrian: Conterminous U.S. (eds. J. C. Reed, Jr., et al.). *Geol. North Am.* **C-2**, 487–517.

Winston D. and Lyons T. W. (1997) Sedimentary cycles in the St. Regis, Empire and Helena formations of the Middle Proterozoic Belt Supergroup, northwestern Montana. In *Geologic Guidebook to the Belt-Purcell Supergroup, Glacier National Park and Vicinity, Montana and Adjacent Canada, Belt Symposium III Field Trip Guidebook (2nd ed.),* (ed. P. K. Link), pp. 21–51. Belt Association, Inc.

Wortmann U. G., Bernasconi S. M., and Böttcher M. E. (2001) Hypersulfidic deep biosphere indicates extreme sulfur isotope fractionation during single-step microbial sulfate reduction. *Geology* **29,** 647–650.

Wrucke C. T. (1989) The Middle Proterozoic Apache Group, Troy Quartzite and associated diabase of Arizona. In *Geologic Evolution of Arizona* (eds. J. P. Jenney and S. J. Reynolds). *Arizona Geol. Soc. Digest* **17,** 239–258.

Zaback D. A., Pratt L. M., and Hayes J. M. (1993) Transport and reduction of sulfate and immobilization of sulfide in marine black shales. *Geology* **21,** 141–144.

Zhang T., Chu X., Zhang Q., Feng L., and Huo Q. (2003) Variations of sulfur and carbon isotopes in seawater during the Doushantuo stage in late Neoproterozoic. *Chinese Sci. Bull.* **48,** 1375–1380.

Zieg G. A. and Leitch C. H. B. (1998) The geology of the Sheep Creek copper deposit, Meagher County, Montana. In *Belt Symposium III Abstracts* (ed. R. B. Berg). *Montana Bur. Mines Geol. Open-File Rpt.* **381**.